Axisymmetric Heat Conduction in a Cracked Layer Subjected to Prescribed Temperatures

Zakaria Baka and Belkacem Kebli

Abstract—This paper presents an analysis of an axisymmetric heat conduction problem in a layer with circular heat sources on its external surfaces, maintaining constant temperatures. Additionally, the layer contains a circular crack along its middle plane, either internally or externally, leading to a mixed boundary value problem. In this study, dual integral equations are derived using Hankel's transform technique. In contrast to the conventional approach that relies on Fredholm's equations, these dual integral equations are directly reduced to an infinite set of simultaneous equations. The investigation subsequently provides closed-form expressions involving special functions for the thermal fields and heat flux intensity factor. Moreover, the solution for the case of a half-space medium is obtained as a limiting case of this study. The accuracy and validity of the present approach are also confirmed through comparison with numerical simulations. Sets of plots are provided to analyze the influence of the crack, surface radius of the applied temperatures, and the layer thickness on various physical quantities.

***Keywords*—Heat conduction, Cracked layer, Mixed boundary value problem, Dual integral equations, Heat flux intensity factor.**

NOMENCLATURE

a	Radius of the heated or cooled area, m.
a_n	Series coefficients.
A, B, C	Unknown functions.
A_{mn}	Matrix elements of the algebraic system.
b	Radius of the penny-shaped crack, m.
b_m	Vector elements of the right-hand side of the algebraic system.
E, K	Complete elliptic integrals of the second and first kinds.
h	Half thickness of the layer, m.
J_ν	Bessel function of the first kind of order ν.
k	Thermal conductivity, $\mathrm{W/(m\,K)}$.
K_T, K'_T	Heat flux intensity factors, $\mathrm{W/m^{3/2}}$.
q_r, q_z	Heat fluxes in the r- and z-directions, $\mathrm{W/m^2}$.
r, z	Radial and axial coordinates, m.
si	Sine integral function.
T	Temperature, K.
T_0	Constant temperature, K.
T_n, U_n	Chebyshev's polynomials of the first and second kinds of degree n.

Greek symbols

α_n	Series coefficients.
δ	Dirac delta function.
$\delta_{\ell m}$	Kronecker delta.
ρ, ζ	Dimensionless radial and axial coordinates.

Manuscript received September 25, 2023; revised December 17, 2024.

Z. Baka and B. Kebli are affiliated with the Laboratory of Green and Mechanical Development (LGMD), Department of Mechanical Engineering, Ecole Nationale Polytechnique (ENP), El-Harrach, 16200 Algiers, ALGERIA (e-mails: zakaria.baka@g.enp.edu.dz, belkacem.kebli@g.enp.edu.dz).

Digital Object Identifier (DOI): 10.53907/enpesj.v4i2.242

I. INTRODUCTION

The study of heat conduction phenomena in solids has significant practical importance in various engineering disciplines, including electronic equipment cooling, aerospace technology, and the nuclear industry. Moreover, the obtained solutions are crucial for determining thermal displacements and stresses in related thermoelastic problems. Several pertinent literature sources, such as [1–3], offer comprehensive insights into the mathematical modeling of heat conduction, providing valuable resources for further exploration of the subject matter. Over the past decades, mixed boundary value problems, where different conditions are applied to distinct regions of the same boundary, have garnered considerable attention in the field of heat conduction. The presence of singularities in these problems often complicates the derivation of solutions using traditional methods, posing significant challenges to researchers. Several researchers have made notable contributions to addressing these challenges. For instance, Dhaliwal [4, 5] investigated heat conduction problems in a slab and effectively reduced the resulting equations to Fredholm equations. He then obtained the solution by employing the successive approximation method. Beck [6] examined the case of a half-space body exposed to a uniform heat flux over a circular area and derived an exact series expression for temperatures. Mehta and Bose [7] studied the steady-state temperature field in a layer subjected to a constant flux over a circular area, presenting a series solution expressed in terms of the Gauss hypergeometric function. The steady-state heat conduction problem in a semi-infinite medium under radiation conditions is addressed by Gladwell et al. [8]. They transformed the cases into integro-differential equations and further simplified them into a set of simultaneous equations. Additionally, many authors have focused on studying thermal constriction resistance [9–13]. Cracked solids present specific challenges, prompting various investigations aimed at enhancing our understanding of heat conduction phenomena and the impact of cracks on the thermal behavior of solids. The majority of these studies have been conducted within the context of thermoelasticity [14–18]. Notably,

Sih [19] was first determined that the temperature gradient or heat flux in the vicinity of the crack tip follows an inverse square-root singularity. Building upon this pioneering work, subsequent researchers have further explored this singularity behavior, employing diverse analytical and numerical methods [20–25]. With the progress of computer technology, numerical methods have experienced significant advancements. However, challenges related to mesh optimization, computation time, and accuracy persist. On the other hand, despite the difficulties involved in constructing mathematical models in theoretical research, analytical techniques continue to be extensively employed. These techniques provide valuable alternatives for investigating solutions in several fields, including heat conduction in cracked solids, and offer distinct advantages compared to numerical approaches. In this context, we aim to investigate the steady-state heat conduction in a cracked layer subjected to circular heat sources with constant temperatures. We consider two types of circular cracks, namely internal and external cracks. The two problems are reduced to a mixed boundary value problem, which we address by employing the Hankel transform technique. This enables us to derive dual integral equations. Using the Gegenbauer addition formula and several integral relations, we simplify these equations into an infinite set of simultaneous equations. Our analysis yields explicit expressions for temperature, heat fluxes, and the flux intensity factor. Additionally, we derive the solution for a semi-infinite medium without cracks as a limiting case. We also validate our results through a finite element simulation using ANSYS software. Selected results are presented graphically, providing insights into the behavior and characteristics of the heat conduction process in solids when cracks are present.

II. Formulation of the Problem

As Fig. 1 shows, the physical domain of interest is a layer with a thickness of $2\,h$, subjected to prescribed temperatures and containing either a penny-shaped crack or an external crack. The penny-shaped crack is assumed to be thermally insulated, whereas the external crack surfaces are maintained at the reference temperature, $T = 0$. An axisymmetric cylindrical coordinate system $(r,\, z)$ is adopted, such that the penny-shaped crack lies in the circular region $r \le b$, positioned at a depth h from the external surface of the layer. In contrast, the external crack is situated in the opposite region $(r \ge b,\, z = h)$. With regards to the thermal properties, the solid is considered homogeneous and isotropic, with a thermal conductivity denoted as k.

In the first case involving the presence of a penny-shaped crack within the layer, as depicted in Fig. 1(a), the temperatures within a circular region of radius a on both the lower and upper surfaces of the layer are assumed to remain constant at T_0 and $-T_0$, respectively. Conversely, in the second case, involving an external crack, the disc-shaped heat sources are both imposing an identical constant temperature T_0, as shown in Fig. 1(b). Additionally, the remaining surfaces in both cases are kept at the reference temperature $(T = 0)$.

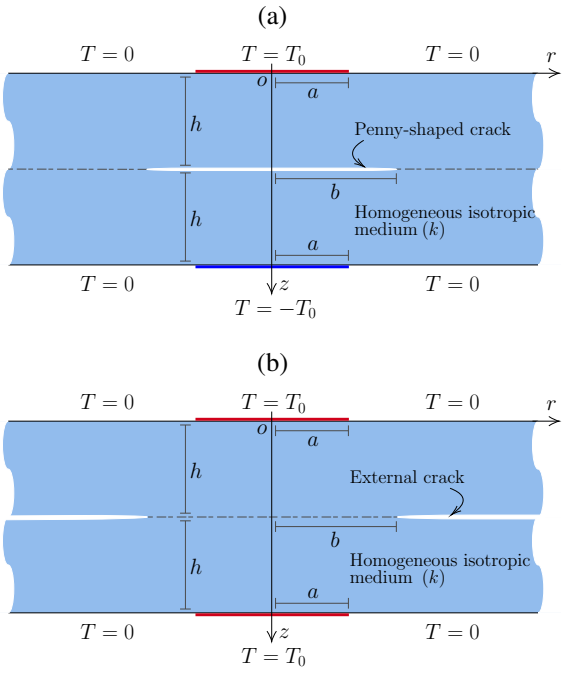

Fig. 1: A layer medium containing (a) an insulated penny-shaped crack; (b) an external crack.

Under the assumption of steady-state thermal loading, and with no heat generation assumed in the medium, the governing equation describing the temperature change T for the considered problems is given as

$$\nabla^2 T(r,z) = 0, \qquad \nabla^2 \equiv \frac{\partial^2}{\partial r^2} + \frac{1}{r}\frac{\partial}{\partial r} + \frac{\partial^2}{\partial z^2}, \tag{1}$$

where ∇^2 represents Laplace's operator expressed in the axisymmetric cylindrical coordinate system.

Since the first problem exhibits anti-symmetry and the second displays symmetry with respect to the plane $z = 0$, we can focus our investigation on the analysis of the half-layer $0 \le z \le h$ of the medium. Thus, both problems can be simplified into the single mixed boundary value problem depicted in Fig. 2.

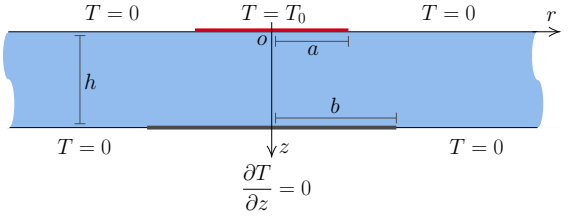

Fig. 2: Geometry of the considered mixed boundary value problem.

This heat conduction problem is governed by (1), which is subject to the following boundary conditions

$$T(r,0) = \begin{cases} T_0, & r \le a, \\ 0, & r > a, \end{cases} \tag{2a}$$

$$\frac{\partial T}{\partial z}(r,h) = 0, \qquad r < b, \tag{2b}$$

$$T(r,h) = 0, \qquad r \ge b. \tag{2c}$$

Furthermore, the regularity conditions require the thermal fields to approach zero as r tends toward infinity $(r \to \infty)$.

III. Analytical solution

This section presents the solution methodology for the mixed boundary value problem illustrated in Fig. 2. The proposed solution scheme involves the derivation of integral dual equations, which are subsequently reduced to an infinite system of algebraic equations. Explicit analytical expressions for the thermal fields and heat flux intensity factor can then be derived based on the solution of the algebraic equations.

A. Derivation of the dual integral equations

To effectively solve the considered problem, it is convenient to use the Hankel integral transform technique, which is particularly well-suited for problems with axisymmetric cylindrical configurations. Specifically, the direct and inverse zeroth-order Hankel transforms of a given function, denoted by f, with respect to the radial variable r, are defined by [26, Eqs. (7.2.8) and (7.2.10)]

$$f_H(\xi) = \int_0^\infty r\, f(r)\, J_0(\xi\, r)\, \mathrm{d}r, \tag{3a}$$

$$f(r) = \int_0^\infty \xi\, f_H(\xi)\, J_0(r\,\xi)\, \mathrm{d}\xi, \tag{3b}$$

respectively, where J_0 stands for the zeroth-order Bessel function of the first kind, and ξ represents the transformed variable. Accordingly, by applying the Hankel transform to the Laplace equation (1), yields

$$\frac{\partial^2 T_H}{\partial z^2}(\xi, z) - \xi^2\, T_H(\xi, z) = 0, \tag{4}$$

which is a second-order ordinary differential equation within T_H represents the Hankel transform counterpart of the temperature T. Considering the boundary condition at infinity, the general solution of (4) can be expressed in the following form

$$T_H(\xi, z) = \frac{\cosh(z\,\xi)\, A(\xi) + \sinh(z\,\xi)\, B(\xi)}{\xi}, \tag{5}$$

where A and B represent unknown functions in terms of ξ to be determined through the boundary conditions.

Applying the Hankel transform to the boundary condition (2a), gives

$$T_H(\xi, 0) = T_0 \int_0^a r\, J_0(\xi\, r)\, \mathrm{d}r. \tag{6}$$

Thus, using the expression for T_H given by (5) and the relation specified in [27, Eq. (5.56 2)], which states that $\int x\, J_0(x)\, \mathrm{d}x = x\, J_1(x)$, we find

$$A(\xi) = a\, T_0\, J_1(a\,\xi). \tag{7}$$

Substituting (7) in (5), one obtains

$$T_H(\xi, z) = \frac{\sinh(z\,\xi)\, B(\xi) + a\, T_0\, \cosh(z\,\xi)\, J_1(a\,\xi)}{\xi}. \tag{8}$$

Consequently, the number of unknown functions is reduced.

Thereafter, we can perform the Hankel inversion transform (3b) on (8), yielding the following expression for the temperature T

$$T = \int_0^\infty \big[\sinh(z\,\xi)\, B(\xi) + a\, T_0\, \cosh(z\,\xi)\, J_1(a\,\xi)\big]\, J_0(r\,\xi)\, \mathrm{d}\xi. \tag{9}$$

To simplify the notation used in this paper, we have not explicitly mentioned the dependence of the functions on the variables (r, z) throughout the text. Nevertheless, this dependence should be understood implicitly.

Continuing with the derivation, we can obtain the temperature gradient by differentiating (9) with respect to z, giving us the expression below

$$\frac{\partial T}{\partial z} = \int_0^\infty \xi \big[\cosh(z\,\xi) B(\xi) + a\, T_0 \sinh(z\,\xi) J_1(a\,\xi)\big]\, J_0(r\,\xi)\, \mathrm{d}\xi. \tag{10}$$

Inserting (10) and (9) into the respective boundary conditions (2b) and (2c), yields

$$\int_0^\infty \xi\, \big[\cosh(h\,\xi)\, B(\xi) + a\, T_0\, \sinh(h\,\xi) \times J_1(a\,\xi)\big]\, J_0(r\,\xi)\, \mathrm{d}\xi = 0, \qquad r < b, \tag{11a}$$

$$\int_0^\infty \big[\sinh(h\,\xi)\, B(\xi) + a\, T_0\, \cosh(h\,\xi) \times J_1(a\,\xi)\big]\, J_0(r\,\xi)\, \mathrm{d}\xi = 0, \qquad r \geq b. \tag{11b}$$

To simplify the latter integral equations, we introduce the function C as follows

$$C(\xi) = \sinh(h\,\xi)\, B(\xi) + a\, T_0\, \cosh(h\,\xi)\, J_1(a\,\xi). \tag{12}$$

Then, B can be expressed in terms of C as

$$B(\xi) = \operatorname{csch}(h\,\xi)\, C(\xi) - a\, T_0\, \coth(h\,\xi)\, J_1(a\,\xi), \tag{13}$$

where $\operatorname{csch}(h\,\xi) = 1/\sinh(h\,\xi)$. Replacing B in (11) with its expression given by (13), and after some algebraic manipulation, we finally get

$$\int_0^\infty \xi \coth(h\,\xi)\, C(\xi)\, J_0(r\,\xi)\, \mathrm{d}\xi = a\, T_0 \int_0^\infty \xi \operatorname{csch}(h\,\xi)\, J_0(r\,\xi)\, J_1(a\,\xi)\, \mathrm{d}\xi, \qquad r < b, \tag{14a}$$

$$\int_0^\infty C(\xi)\, J_0(r\,\xi)\, \mathrm{d}\xi = 0, \qquad r \geq b. \tag{14b}$$

Equations (14a) and (14b) form dual integral equations for determining the unknown function C.

B. Solution of the dual integral equations

Our task turns to determine the unknown function C through the system of dual integral equations (14). To solve such kinds of integral equations with Bessel function kernels, several approaches can be employed, including those used by Sneddon [28, 29], Duffy [30], Sakamoto [31], Kebli and Madani [32]. Among these approaches, the one presented in [31] has the advantage of reducing the system of triple integral equations directly into the solution of an infinite system of algebraic equations. This approach, along with similar methods, have been increasingly utilized in recent studies to solve diverse mixed boundary value problems [33–37], indicating the broad range of applicability of such techniques.

Therefore, in this work, we adopt the solution approach outlined by Sakamoto [31] and use the following dual integral formula [37, Eq. (A4)]

$$\int_0^\infty N_n(\xi)\, J_0(r\,\xi)\, \mathrm{d}\xi = \begin{cases} \dfrac{4\sqrt{b^2 - r^2}}{\pi\, b^2\, r}\, U_{2\,n+1}(r/b), & r < b, \\ 0, & r > b, \end{cases} \tag{15}$$

where $n = 0, 1, 2, \ldots$, $N_n(\xi) = \xi\,[M_n(\xi) - M_{n+1}(\xi)]$ and $M_n(\xi) = J_{n+1/2}(b\,\xi/2)\,J_{-(n+1/2)}(b\,\xi/2)$. Additionally, U_n is the Chebyshev polynomials of the second kind of degree n. They are defined by the relation $U_n(x) = \sin[(n+1)\arccos x]/\sin[\arccos x]$ [27, Eq. (8.940 2)].

Accordingly, we express the function C as a series expansion involving Bessel functions in the following form

$$C(\xi) = a\,T_0 \sum_{n=0}^{\infty} a_n\,N_n(\xi), \tag{16}$$

where a_n are unknown coefficients to be determined later. By adopting this expression, we can readily deduce that (14b) is automatically satisfied, as indicated by (15). Then, inserting (16) into (14a), yields

$$\sum_{n=0}^{\infty} a_n \int_0^{\infty} \xi \coth(h\,\xi)\,N_n(\xi)\,J_0(r\,\xi)\,\mathrm{d}\xi = \int_0^{\infty} \xi\,\mathrm{csch}(h\,\xi)\,J_0(r\,\xi)\,J_1(a\,\xi)\,\mathrm{d}\xi, \qquad r < b. \tag{17}$$

In order to eliminate the radial variable r, we can utilize the Gegenbauer addition formula below [27, Eq. (8.531 3)]

$$J_0(r\,\xi) = \sum_{m=0}^{\infty} (2 - \delta_{0m})\,X_m(\xi)\,\cos(m\,\phi), \qquad r < b, \tag{18}$$

where $X_m(\xi) = J_m^2(b\,\xi/2)$, $\phi = 2\arcsin(r/b)$ and $\delta_{\ell m}$ stands for the Kronecker delta, which is defined by $\delta_{\ell m} = \begin{cases} 1, & \ell = m, \\ 0, & \ell \neq m. \end{cases}$

By substituting (18) into (17), rearranging the terms, and interchanging the order of integration and summation, we get

$$\sum_{m=0}^{\infty} (2-\delta_{0m})\cos(m\,\phi) \sum_{n=0}^{\infty} a_n \int_0^{\infty} \xi \coth(h\,\xi) N_n(\xi) X_m(\xi)\,\mathrm{d}\xi = \sum_{m=0}^{\infty} (2-\delta_{0m})\cos(m\,\phi) \int_0^{\infty} \xi\,\mathrm{csch}(h\,\xi)\,X_m(\xi)\,J_1(a\,\xi)\,\mathrm{d}\xi. \tag{19}$$

Thereafter, by matching the coefficients of $\cos(m\,\phi)$ on both sides of (19), we obtain the following infinite set of simultaneous equations

$$\sum_{n=0}^{\infty} a_n \int_0^{\infty} \xi \coth(h\,\xi)\,N_n(\xi)\,X_m(\xi)\,\mathrm{d}\xi = \int_0^{\infty} \xi\,\mathrm{csch}(h\,\xi)\,X_m(\xi)\,J_1(a\,\xi)\,\mathrm{d}\xi, \tag{20}$$

where $m = 0, 1, 2, \ldots$

In order to get a symmetric coefficient matrix and accelerate the convergence of the previous algebraic system, we subtract the $(m+2)$th equations from the mth equations in (20). As a result, we arrive at an algebraic system for determining a_n, expressed in matrix form as follows

$$\sum_{n=0}^{\infty} A_{mn}\,a_n = b_m, \qquad m = 0, 1, 2, \ldots \tag{21}$$

where $A_{mn} = \int_0^{\infty} \coth(h\,\xi)\,N_n(\xi)\,Y_m(\xi)\,\mathrm{d}\xi$, $Y_m(\xi) = \xi\,[X_m(\xi) - X_{m+2}(\xi)]$ and $b_m = \int_0^{\infty} \mathrm{csch}(h\,\xi)\,Y_m(\xi)\,J_1(a\,\xi)\,\mathrm{d}\xi$.

Consequently, we have effectively reduced the heat conduction problems under consideration to solving an infinite set of simultaneous equations defined by (21). Notably, this system depends only on the geometric parameters a, b and h.

C. Temperature and heat flux expressions

We now proceed to derive the expressions for temperature and heat fluxes in terms of the series coefficients a_n. By considering (13) and (16), we can explicitly express the temperature field described by equation (9) as follows

$$T = a\,T_0 \left\{ \int_0^{\infty} \mathrm{csch}(h\,\xi)\sinh((h-z)\,\xi) J_0(r\,\xi)\,J_1(a\,\xi)\,\mathrm{d}\xi + \sum_{n=0}^{\infty} a_n \int_0^{\infty} \mathrm{csch}(h\,\xi)\,\sinh(z\,\xi)\,N_n(\xi)\,J_0(r\,\xi)\,\mathrm{d}\xi \right\}. \tag{22}$$

Furthermore, following the Fourier law of heat conduction, the heat flux in the r- and z-directions can be expressed as $q_r = -k\,\partial T/\partial r$ and $q_z = -k\,\partial T/\partial z$, respectively. Consequently, their expressions in terms of a_n can be obtained. Formally,

$$q_r = a\,k\,T_0 \left\{ \int_0^{\infty} \xi\,\mathrm{csch}(h\,\xi)\,\sinh((h-z)\,\xi)\,J_1(a\,\xi) J_1(r\,\xi)\,\mathrm{d}\xi + \sum_{n=0}^{\infty} a_n \int_0^{\infty} \xi\,\mathrm{csch}(h\,\xi)\,\sinh(z\,\xi)\,N_n(\xi)\,J_1(r\,\xi)\,\mathrm{d}\xi \right\}, \tag{23a}$$

$$q_z = a\,k\,T_0 \left\{ \int_0^{\infty} \xi\,\mathrm{csch}(h\,\xi)\cosh((h-z)\,\xi)\,J_0(r\,\xi) J_1(a\,\xi)\,\mathrm{d}\xi - \sum_{n=0}^{\infty} a_n \int_0^{\infty} \xi\,\mathrm{csch}(h\,\xi)\cosh(z\,\xi)\,N_n(\xi)\,J_0(r\,\xi)\,\mathrm{d}\xi \right\}. \tag{23b}$$

The planes $z = 0$ and $z = h$ are of particular interest. When considering the case where $z = 0$, the previously mentioned heat flux expressions can be rewritten as

$$q_r(r,0) = a\,k\,T_0 \int_0^{\infty} \xi\,J_1(a\,\xi)\,J_1(r\,\xi)\,\mathrm{d}\xi, \tag{24a}$$

$$q_z(r,0) = a\,k\,T_0 \left\{ \int_0^{\infty} \xi \coth(h\,\xi)\,J_0(r\,\xi)\,J_1(a\,\xi)\,\mathrm{d}\xi - \sum_{n=0}^{\infty} a_n \int_0^{\infty} \xi\,\mathrm{csch}(h\,\xi)\,N_n(\xi)\,J_0(r\,\xi)\,\mathrm{d}\xi \right\}. \tag{24b}$$

From the identity given by [27, Eq. (6.512 8)], we have

$$\int_0^{\infty} \xi\,J_1(a\,\xi)\,J_1(r\,\xi)\,\mathrm{d}\xi = \delta(r-a)/a, \tag{25}$$

where δ denotes the Dirac delta function, defined by

$$\delta(x) = \begin{cases} \infty, & x = 0, \\ 0, & x \neq 0. \end{cases} \tag{26}$$

Here, it is worth mentioning that the Dirac delta function is frequently employed in problems involving concentrated loads or local sources [3, ch. 9].

By making use of (25) and (A.6), we can finally express the heat fluxes at the plane $z = 0$ as follows

$$q_r(r,0) = k\,T_0\,\delta(r-a), \tag{27a}$$

$$q_z(r,0) = a\,k\,T_0 \left\{ \int_0^{\infty} \xi\,[\coth(h\,\xi) - 1]\,J_0(r\,\xi)\,J_1(a\,\xi)\,\mathrm{d}\xi - \frac{1}{\pi\,a}\left[\frac{E\left(\frac{2\sqrt{a\,r}}{r+a}\right)}{r-a} - \frac{K\left(\frac{2\sqrt{a\,r}}{r+a}\right)}{r+a} \right] - \sum_{n=0}^{\infty} a_n \int_0^{\infty} \xi\,\mathrm{csch}(h\,\xi)\,N_n(\xi)\,J_0(r\,\xi)\,\mathrm{d}\xi \right\}, \tag{27b}$$

where K and E represent the complete elliptic integrals of the first and second kinds, respectively. They are given as [27, p. 396]

$$K(y) = \int_0^{\pi/2} \frac{\mathrm{d}x}{\sqrt{1 - y^2\,\sin^2 x}}, \tag{28a}$$

$$E(y) = \int_0^{\pi/2} \sqrt{1 - y^2\,\sin^2 x}\,\mathrm{d}x. \tag{28b}$$

Regarding the plane $z = h$, by setting $z = h$ in (22) and (23), we get

$$T(r,h) = a\,T_0 \sum_{n=0}^{\infty} a_n \int_0^{\infty} N_n(\xi)\,J_0(r\,\xi)\,\mathrm{d}\xi, \tag{29a}$$

$$q_r(r,h) = a\,k\,T_0 \sum_{n=0}^{\infty} a_n \int_0^{\infty} \xi\,N_n(\xi)\,J_1(r\,\xi)\,\mathrm{d}\xi, \tag{29b}$$

$$\begin{aligned} q_z(r,h) = a\,k\,T_0 \Bigg\{ &\int_0^{\infty} \xi\,\mathrm{csch}(h\,\xi) J_0(r\,\xi) J_1(a\,\xi)\,\mathrm{d}\xi \\ &- \sum_{n=0}^{\infty} a_n \int_0^{\infty} \xi\,\coth(h\,\xi)\,N_n(\xi)\,J_0(r\,\xi)\,\mathrm{d}\xi \Bigg\}. \end{aligned} \tag{29c}$$

With the help of (15), (29a) is further simplified to

$$T(r,h) = \frac{4\,a\,T_0\,\sqrt{b^2 - r^2}\,H(b-r)}{\pi\,b^2\,r} \sum_{n=0}^{\infty} a_n\,U_{2\,n+1}(r/b), \tag{30}$$

wherein H denotes the Heaviside step function defined by

$$H(x) = \begin{cases} 0, & x \le 0, \\ 1, & x > 0. \end{cases}$$

As for the heat fluxes, by virtue of (A.16) and (A.28), we obtain the following expressions

$$\begin{aligned} q_r(r,h) = &-\frac{4\,a\,k\,T_0\,H(b-r)}{\pi\,b^2\,r^2\,\sqrt{b^2 - r^2}} \sum_{n=0}^{\infty} a_n \big\{ 2\,(n+1)\,b\,r\,U_{2\,n}(r/b) \\ &- \left[(2\,n+1)\,r^2 + b^2\right] U_{2\,n+1}(r/b) \big\}, \end{aligned} \tag{31a}$$

$$\begin{aligned} q_z(r,h) = &\,a\,k\,T_0\,H(r-b) \\ &\times \Bigg\{ \int_0^{\infty} \xi\,\mathrm{csch}(h\,\xi)\,J_0(r\,\xi)\,J_1(a\,\xi)\,\mathrm{d}\xi - \sum_{n=0}^{\infty} a_n \\ &\times \Bigg[\int_0^{\infty} \left(\xi\,\coth(h\,\xi)\,N_n(\xi) + \frac{8\,(n+1)\cos(b\,\xi)}{\pi\,b^2} \right) \\ &\times J_0(r\,\xi)\,\mathrm{d}\xi - \frac{8\,(n+1)}{\pi\,b^2\sqrt{r^2 - b^2}} \Bigg] \Bigg\}. \end{aligned} \tag{31b}$$

In view of (31), it can be observed that q_r and q_z are proportional to the inverse square-roots $1/\sqrt{b-r}$ and $1/\sqrt{r-b}$, respectively. This indicates that the heat fluxes exhibit the usual square-root singularity in the vicinity of the crack tip b [19–22, 38].

D. The special case of a semi-infinite medium ($h \to \infty$)

As h approaches infinity, this limiting case corresponds to a half-space medium where a circular heat source imposes a uniform temperature, while the rest of the surface is kept at a reference temperature. In this case, the vector elements b_m on the right-hand side of the algebraic system (21) become zero, owing to the limit $\lim_{h\to\infty} \mathrm{csch}(h\,\xi) = 0$. As a result, the algebraic system reduces to the following form

$$\sum_{n=0}^{\infty} A_{mn}\,a_n = 0, \qquad m = 0,\,1,\,2,\,\ldots \tag{32}$$

leading to a trivial solution ($a_n = 0$). Additionally, we have $\lim_{h\to\infty} \sinh((h-z)\,\xi)\,\mathrm{csch}(h\,\xi) = \mathrm{e}^{-z\,\xi}$. This readily simplifies the expressions for the temperature and heat fluxes to

$$T = a\,T_0 \int_0^{\infty} \mathrm{e}^{-z\,\xi}\,J_0(r\,\xi)\,J_1(a\,\xi)\,\mathrm{d}\xi, \tag{33a}$$

$$q_r = a\,k\,T_0 \int_0^{\infty} \xi\,\mathrm{e}^{-z\,\xi}\,J_1(a\,\xi)\,J_1(r\,\xi)\,\mathrm{d}\xi, \tag{33b}$$

$$q_z = a\,k\,T_0 \int_0^{\infty} \xi\,\mathrm{e}^{-z\,\xi}\,J_0(r\,\xi)\,J_1(a\,\xi)\,\mathrm{d}\xi. \tag{33c}$$

These expressions are identical to the exact solution derived in Appendix B.

E. Heat flux intensity factor

As outlined in subsection II.C on page 33, the heat fluxes near the crack tip exhibit a square-root singularity. To quantify the strength of this singularity, a heat flux intensity factor is introduced in an analogous way to the stress intensity factor. The latter plays a crucial role in understanding mechanical and thermal stresses and crack behavior. The heat flux component perpendicular to the crack, in our case, q_z, is more directly related to crack tip behavior and the generation of thermal stresses. Therefore, the heat flux intensity factor, denoted as K_T, pertains to this component, and its definition is given by [38, Eq. (2.3)]

$$K_T = \lim_{r\to b^+} \sqrt{2\,(r-b)}\,q_z(r,h). \tag{34}$$

Upon substitution of the heat flux expression provided by (31b) into the aforementioned equation leads to

$$\begin{aligned} K_T = a\,k\,T_0 \lim_{r\to b^+} \sqrt{2\,(r-b)} \Bigg\{ &\int_0^{\infty} \xi\,\mathrm{csch}(h\,\xi) J_0(r\,\xi) J_1(a\,\xi)\mathrm{d}\xi \\ &- \sum_{n=0}^{\infty} a_n \Bigg[\int_0^{\infty} \Bigg(\xi\,\coth(h\,\xi)\,N_n(\xi) \\ &+ \frac{8\,(n+1)\cos(b\,\xi)}{\pi\,b^2} \Bigg) J_0(r\,\xi)\,\mathrm{d}\xi - \frac{8\,(n+1)}{\pi\,b^2\sqrt{r^2 - b^2}} \Bigg] \Bigg\}. \end{aligned} \tag{35}$$

Within this equation, only the last term is singular. Consequently, this equation readily reduces to

$$K_T = \frac{8\,a\,k\,T_0}{\pi\,b^2\,\sqrt{b}} \sum_{n=0}^{\infty} (n+1)\,a_n. \tag{36}$$

It is worth noting that the heat flux component parallel to the crack is usually not included in standard heat flux intensity factor calculations. Nevertheless, for the sake of completeness, we also derive the heat flux intensity factor related to this component.

Let us denote the heat flux intensity factor associated with q_r as K'_T. Following a similar form as in (34), we can express K'_T as

$$K'_T = \lim_{r\to b^-} \sqrt{2\,(b-r)}\,q_r(r,h). \tag{37}$$

Inserting (31a) into (37), yields

$$\begin{aligned} K'_T = -\frac{4\sqrt{2}\,a\,k\,T_0}{\pi\,b^2} \lim_{r\to b^-} \sum_{n=0}^{\infty} \frac{a_n}{r^2\,\sqrt{r+b}} \big\{ &2\,(n+1)\,b\,r \\ &\times U_{2\,n}(r/b) - \left[(2\,n+1)\,r^2 + b^2\right] U_{2\,n+1}(r/b) \big\}. \end{aligned} \tag{38}$$

We then proceed with the evaluation of the limit using the trigonometric forms of the Chebyshev polynomials U_n and L'Hôpital's rule. We have

$$\lim_{r\to b^-} U_n(r/b) = \lim_{r\to b^-} \frac{\sin\left[(n+1)\arccos(r/b)\right]}{\sin\left[\arccos(r/b)\right]} \tag{39a}$$

$$= \lim_{r\to b^-} \frac{\frac{\mathrm{d}}{\mathrm{d}r}\sin\left[(n+1)\arccos(r/b)\right]}{\frac{\mathrm{d}}{\mathrm{d}r}\sin\left[\arccos(r/b)\right]}. \tag{39b}$$

Performing the differentiation of (39b) with respect to r, we get

$$\lim_{r\to b^-} U_n(r/b) = \lim_{r\to b^-} \frac{(n+1)\,b\,\cos\left[(n+1)\arccos(r/b)\right]}{r}. \tag{40}$$

Thus, $\lim_{r\to b^-} U_n(r/b) = n+1$. Accordingly, upon evaluating the limit in (38), we obtain

$$K_T' = \frac{8\,a\,k\,T_0}{\pi\,b^2\,\sqrt{b}} \sum_{n=0}^{\infty} (n+1)\,a_n. \tag{41}$$

Remarkably, it has been found that the expressions for heat flux intensity factors K_T and K_T' are identical ($K_T = K_T'$). Consequently, our focus in the following discussion will only be on K_T.

F. Dimensionless expressions

Dealing with dimensionless quantities is often convenient. We can achieve this by introducing a variable change $\eta = b\,\xi$. Additionally, the dimensionless parameters $\bar{a} = a/b$, $\bar{h} = h/b$, $\rho = r/b$ and $\zeta = z/b$ are also used. We then express the matrix elements A_{mn} and vector elements b_m as $A_{mn} = \bar{A}_{mn}/b^3$ and $\bar{b}_m = b_m/b^2$. Here, $\bar{A}_{mn}$ and $\bar{b}_m$ are given by

$$\bar{A}_{mn} = \int_0^{\infty} \coth(\bar{h}\,\eta)\,\bar{N}_n(\eta)\,\bar{Y}_m(\eta)\,\mathrm{d}\eta, \tag{42a}$$

$$\bar{b}_m = \int_0^{\infty} \operatorname{csch}(\bar{h}\,\eta)\,\bar{Y}_m(\eta)\,J_1(\bar{a}\,\eta)\,\mathrm{d}\eta, \tag{42b}$$

where $\bar{N}_n(\eta) = b\,N_n(\eta/b)$ and $\bar{Y}_m(\eta) = b\,Y_m(\eta/b)$.

Therefore, by considering $\alpha_n = a_n/b$, the algebraic system (21) can be transformed into the following dimensionless form

$$\sum_{n=0}^{\infty} \bar{A}_{mn}\,\alpha_n = \bar{b}_m, \qquad m = 0,\,1,\,2,\,\ldots \tag{43}$$

As for the dimensionless temperature, fluxes, and heat flux intensity factor, we define them as follows: $\bar{T} = T/T_0$, $\bar{q}_r = b\,q_r/(k\,T_0)$, $\bar{q}_z = b\,q_z/(k\,T_0)$, and $\bar{K}_T = \sqrt{b}\,K_T/(k\,T_0)$. By using these quantities and the previously introduced dimensionless parameters, we can transform the expressions (22), (23), (27), (30), (31) and (36) that represent the thermal fields and heat flux intensity factor into their dimensionless forms.

The dimensionless expressions for temperature are obtained as follows

$$\bar{T}(\rho,\zeta) = \bar{a}\left\{\int_0^{\infty} \operatorname{csch}(\bar{h}\,\eta)\sinh((\bar{h}-\zeta)\,\eta)\,J_0(\rho\,\eta)\,J_1(\bar{a}\,\eta)\,\mathrm{d}\eta + \sum_{n=0}^{\infty}\alpha_n\int_0^{\infty} \operatorname{csch}(\bar{h}\,\eta)\sinh(\zeta\,\eta)\,\bar{N}_n(\eta)\,J_0(\rho\,\eta)\,\mathrm{d}\eta\right\}, \tag{44a}$$

$$\bar{T}(\rho,\bar{h}) = \frac{4\,\bar{a}\,\sqrt{1-\rho^2}\,H(1-\rho)}{\pi\,\rho}\sum_{n=0}^{\infty}\alpha_n\,U_{2\,n+1}(\rho). \tag{44b}$$

The dimensionless expressions for the heat flux in the radial direction can be expressed as

$$\bar{q}_r(\rho,\zeta) = \bar{a}\left\{\int_0^{\infty} \eta\operatorname{csch}(\bar{h}\,\eta)\sinh((\bar{h}-\zeta)\,\eta)\,J_1(\bar{a}\,\eta)\,J_1(\rho\,\eta)\,\mathrm{d}\eta + \sum_{n=0}^{\infty}\alpha_n\int_0^{\infty} \eta\operatorname{csch}(\bar{h}\,\eta)\sinh(\zeta\,\eta)\,\bar{N}_n(\eta)\,J_1(\rho\,\eta)\,\mathrm{d}\eta\right\}, \tag{45a}$$

$$\bar{q}_r(\rho,0) = \delta(\rho-\bar{a}), \tag{45b}$$

$$\bar{q}_r(\rho,\bar{h}) = -\frac{4\,\bar{a}\,H(1-\rho)}{\pi\,\rho^2\,\sqrt{1-\rho^2}}\sum_{n=0}^{\infty}\alpha_n\left\{2\,(n+1)\,\rho\,U_{2\,n}(\rho) - \left[(2\,n+1)\,\rho^2+1\right]U_{2\,n+1}(\rho)\right\}. \tag{45c}$$

Regarding the heat flux in the axial direction, the dimensionless expressions are given by

$$\bar{q}_z(\rho,\zeta) = \bar{a}\left\{\int_0^{\infty} \eta\operatorname{csch}(\bar{h}\,\eta)\cosh((\bar{h}-\zeta)\,\eta)\,J_0(\rho\,\eta)\,J_1(\bar{a}\,\eta)\,\mathrm{d}\eta - \sum_{n=0}^{\infty}\alpha_n\int_0^{\infty} \eta\operatorname{csch}(\bar{h}\,\eta)\cosh(\zeta\,\eta)\,\bar{N}_n(\eta)\,J_0(\rho\,\eta)\,\mathrm{d}\eta\right\}, \tag{46a}$$

$$\bar{q}_z(\rho,0) = \bar{a}\left\{\int_0^{\infty} \eta\left[\coth(\bar{h}\,\eta)-1\right]J_0(\rho\,\eta)\,J_1(\bar{a}\,\eta)\,\mathrm{d}\eta - \frac{1}{\pi\,\bar{a}}\left[\frac{E\left(\frac{2\sqrt{\bar{a}\,\rho}}{\rho+\bar{a}}\right)}{\rho-\bar{a}} - \frac{K\left(\frac{2\sqrt{\bar{a}\,\rho}}{\rho+\bar{a}}\right)}{\rho+\bar{a}}\right] - \sum_{n=0}^{\infty}\alpha_n\int_0^{\infty} \eta\operatorname{csch}(\bar{h}\,\eta)\,\bar{N}_n(\eta)\,J_0(\rho\,\eta)\,\mathrm{d}\eta\right\}, \tag{46b}$$

$$\bar{q}_z(\rho,\bar{h}) = \bar{a}\,H(\rho-1)\times\left\{\int_0^{\infty} \eta\operatorname{csch}(\bar{h}\,\eta)\,J_0(\rho\,\eta)\,J_1(\bar{a}\,\eta)\,\mathrm{d}\eta - \sum_{n=0}^{\infty}\alpha_n \times\left[\int_0^{\infty}\left(\eta\coth(\bar{h}\,\eta)\,\bar{N}_n(\eta) + \frac{8\,(n+1)\cos(\eta)}{\pi}\right)\times J_0(\rho\,\eta)\,\mathrm{d}\eta - \frac{8\,(n+1)}{\pi\,\sqrt{\rho^2-1}}\right]\right\}. \tag{46c}$$

Finally, the expression for the dimensionless heat flux intensity factor can be written as

$$\bar{K}_T = \frac{8\,\bar{a}}{\pi}\sum_{n=0}^{\infty}(n+1)\,\alpha_n. \tag{47}$$

IV. Numerical Results and Discussion

In the preceding section, we derived explicit expressions for the temperature, heat fluxes, and heat flux intensity factor, all of which are presented in dimensionless form in (44)-(47). In this section, we perform numerical calculations using these expressions to illustrate the thermal fields and analyze the influence of various parameters on these quantities. Furthermore, to validate the obtained results, a numerical simulation is conducted using finite element method (ANSYS software).

A. Numerical scheme

The thermal field variables and heat flux intensity factor are expressed in terms of the coefficients α_n, which are the solution of

the algebraic system (43). Therefore, the calculation of these coefficients is crucial for further analysis of the involved physical quantities. To achieve this, we solve the algebraic system (43) using the truncation method [39, 40]. This approach involves selecting an appropriate finite number of equations from the system to solve, enabling us to obtain solutions for the coefficients α_n.

However, the analytical computation of the coefficient matrix elements $\bar{A}_{mn}$ and vector elements $\bar{b}_m$ poses a significant challenge due to their representation as infinite integrals (42a) and (42b), respectively. Therefore, we resort to numerical integration procedures. In this regard, we integrate $\bar{A}_{mn}$ in two steps: from 0 to a sufficiently large number, denoted as η_0, and from η_0 to infinity. Formally,

$$\bar{A}_{mn} = \int_0^{\eta_0} \coth(\bar{h}\,\eta)\,\bar{N}_n(\eta)\,\bar{Y}_m(\eta)\,\mathrm{d}\eta + A'_{mn}, \tag{48}$$

where A'_{mn} corresponds to the integral from η_0 to infinity. The evaluation of the first integral can be accomplished by utilizing an appropriate numerical method. The value of η_0 must be chosen sufficiently large to ensure that the term $\coth(\bar{h}\,\eta)$ approaches one. This allows us to approximate the improper integral A'_{mn} as

$$A'_{mn} \simeq \int_{\eta_0}^{\infty} \bar{N}_n(\eta)\,\bar{Y}_m(\eta)\,\mathrm{d}\eta. \tag{49}$$

Moreover, η_0 should also be sufficiently large to enable the effective use of the asymptotic expansion of Bessel functions. For example, a value of $\eta_0 = 5000$ may be used. Consequently, A'_{mn} can be evaluated through the expression

$$A'_{mn} \simeq \frac{128\,(-1)^m\,(m+1)\,(n+1)}{\pi^2}\left[\frac{\cos(\eta_0)^2}{\eta_0} + \mathrm{si}(2\,\eta_0)\right], \tag{50}$$

which is derived in Appendix A.*C*. In the above relation, si is the sine integral function defined by [27, Eq. (8.230 1)]

$$\mathrm{si}(x) = -\int_x^{\infty} \frac{\sin t}{t}\,\mathrm{d}t. \tag{51}$$

Regarding the infinite integral $\bar{b}_m$, it is worth noting that the term $\mathrm{csch}(\bar{h}\,\eta)$ rapidly decreases and approaches zero as η tends to infinity. Furthermore, based on the asymptotic expressions of Bessel's functions and $\bar{Y}_m(\eta)$ given by (A.18) and (A.21b), respectively, we can determine that $\bar{b}_m$ is a convergent integral. Consequently, we can evaluate it using an appropriate numerical method as

$$\bar{b}_m \simeq \int_0^{\eta_0} \mathrm{csch}(\bar{h}\,\eta)\,\bar{Y}_m(\eta)\,J_1(\bar{a}\,\eta)\,\mathrm{d}\eta. \tag{52}$$

By employing the aforementioned approximation scheme, we can effectively solve an appropriately truncated system of the algebraic system (43) with adequate accuracy. The first ten terms of α_n are presented in Tables I and II for various values of $\bar{a}$ and $\bar{h}$. One can observe that the coefficients exhibit rapid convergence. However, as $\bar{a}$ or $\bar{h}$ decrease, the convergence becomes slower. Nonetheless, extensive testing has shown that considering less than ten terms of the coefficients in the calculations is generally sufficient for generating convergent results in most practical cases, as shown in Table III.

Table. I

FIRST TENTH TERMS OF THE COEFFICIENTS α_n FOR VARIOUS VALUES OF $\bar{a}$ WITH $\bar{h} = 0.75$

	$\bar{h} = 0.75$			
n	$\bar{a} = 0.25$	$\bar{a} = 0.5$	$\bar{a} = 1$	$\bar{a} = 2$
0	0.069516	0.133246	0.202032	0.142320
1	−0.022279	−0.033799	−0.017122	0.001066
2	0.006137	0.006334	−0.000630	−0.000118
3	−0.001516	−0.000792	0.000215	−0.000001
4	0.000343	0.000022	0.000005	0.000000
5	−0.000071	0.000020	−0.000004	0.000000
6	0.000013	−0.000006	0.000000	0.000000
7	−0.000002	0.000001	0.000000	0.000000
8	0.000000	0.000000	0.000000	0.000000
9	0.000000	0.000000	0.000000	0.000000

Table. II

FIRST TENTH TERMS OF THE COEFFICIENTS α_n FOR VARIOUS VALUES OF $\bar{h}$ WITH $\bar{a} = 1.5$

	$\bar{a} = 1.5$			
n	$\bar{h} = 0.25$	$\bar{h} = 0.5$	$\bar{h} = 1$	$\bar{h} = 2$
0	0.324641	0.242438	0.134396	0.046306
1	0.034327	0.005770	−0.002950	−0.001347
2	0.000721	−0.000752	−0.000214	0.000015
3	−0.000479	−0.000058	0.000004	0.000001
4	−0.000037	−0.000002	0.000001	0.000000
5	0.000010	0.000000	0.000000	0.000000
6	0.000001	0.000000	0.000000	0.000000
7	0.000000	0.000000	0.000000	0.000000
8	0.000000	0.000000	0.000000	0.000000
9	0.000000	0.000000	0.000000	0.000000

Table. III

EXAMPLES OF NUMERICAL VALUES FOR DIMENSIONLESS THERMAL FIELDS AGAINST THE NUMBER OF TERMS USED IN THE CALCULATION.

$\bar{a}$	$\bar{h}$	ρ	ζ	m, n	$\bar{T}(\rho,\zeta)$	$\bar{q}_r(\rho,\zeta)$	$\bar{q}_z(\rho,\zeta)$
0.25	0.5	0.5	0.25	2	0.059183	0.267378	−0.078051
				4	0.063323	0.297678	−0.090873
				6	0.063718	0.299169	−0.091553
				8	0.063754	0.299283	−0.091693
				10	0.063753	0.299281	−0.091691
				15	0.063753	0.299281	−0.091691
0.5	1.5	1	0.75	2	0.044434	0.098666	0.028904
				4	0.044479	0.098762	0.028855
				6	0.044480	0.098763	0.028855
				8	0.044480	0.098763	0.028855
				10	0.044480	0.098763	0.028855
				15	0.044480	0.098763	0.028855
1	1.25	0.5	1	2	0.259398	0.219466	0.217509
				4	0.259694	0.220796	0.217074
				6	0.259692	0.220791	0.217074
				8	0.259692	0.220791	0.217074
				10	0.259692	0.220791	0.217074
				15	0.259692	0.220791	0.217074
2	0.75	1.5	0.25	2	0.631150	0.217688	1.395149
				4	0.631147	0.217675	1.395158
				6	0.631147	0.217675	1.395158
				8	0.631147	0.217675	1.395158
				10	0.631147	0.217675	1.395158
				15	0.631147	0.217675	1.395158

Once the coefficients α_n are determined, the thermal fields and heat flux intensity factor can be obtained from (44)-(47). It is important to note that the asymptotic expansions of Bessel's functions and $\bar{N}_n(\eta)$ (Eqs. A.18 and A.21a) provided in Appendix A, combined with the decreasing nature of the weight functions, guarantee the convergence of the integrals involved in the expressions for temperature and heat fluxes. Consequently, these integrals can be evaluated with a suitable level of accuracy using an appropriate numerical method.

B. Finite element modeling and comparison with the present results

For the sake of validating the solution obtained by the present method, we carry out a numerical simulation of the temperature field using ANSYS Workbench software. Figure 3 displays the finite element model along with the imposed boundary conditions. Here, we adopt the dimensionless forms of the coordinates, geometric parameters, temperature and heat fluxes, as established in subsection II.*F*. Due to the axisymmetric property of the problem, we only consider its projection onto the (ρ, ζ) plane.

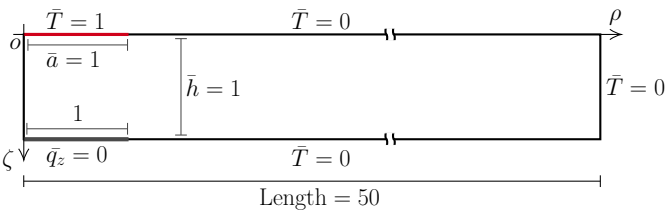

Fig. 3: Geometry and boundary conditions of the finite element model.

The geometric parameters are taken as $\bar{a} = \bar{h} = 1$, while the length extends to 50. This specific length value is intentionally chosen to ensure that the computational results remain unaffected by this factor. Concerning boundary conditions, we impose the conditions prescribed in section II. Additionally, the temperatures on the boundary $\rho = 50$ are set to zero, and the software automatically applies boundary conditions on the symmetry axis $\rho = 0$.

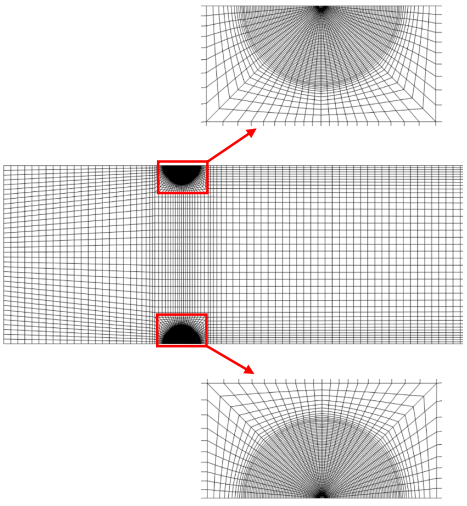

Fig. 4: Typical finite element mesh used for the analysis of heat conduction in a layer.

For the sake of discretization, the geometry is divided into quadrilateral elements, with a typical length of 0.04. Furthermore, triangular singular elements are used, and the mesh has been refined near points where $\rho = 1$, $\zeta = 0$ and $\zeta = 1$ to accurately model temperature gradients and heat fluxes in these critical regions. A visual representation of a typical mesh used in the model is depicted in Fig. 4.

Figure 5 compares the radial distribution of the dimensionless temperature $\bar{T}$ at different ζ-plane ($\zeta = 0.25$, 0.5, 0.75, and 1). As shown, the analytical and numerical results are in good agreement, thereby validating the present analysis.

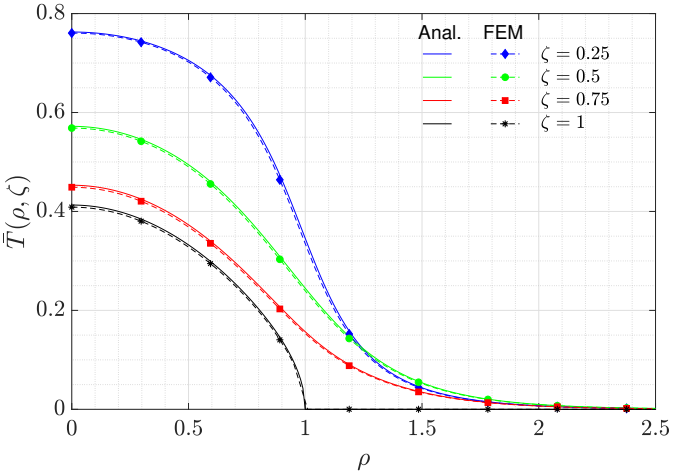

Fig. 5: Radial distribution of the dimensionless temperature $\bar{T}$ for various values of ζ with $\bar{a} = \bar{h} = 1$, as obtained by the present analytical approach and the numerical simulation.

C. Thermal fields

The expressions (44)-(46) enable us to calculate the temperature and heat flux fields within the region $0 \le \zeta \le \bar{h}$ of the medium. Furthermore, the symmetry characteristics with respect to the crack plane $\zeta = 0$, which are inherent in the studied problems, require:

- For the first problem, which involves a penny-shaped crack as shown in Fig. 1(a), $\bar{T}$ and $\bar{q}_r$ should exhibit anti-symmetry, while $\bar{q}_z$ should be symmetric.
- In the case of an external crack, representing the second problem as depicted in Fig. 1(b), $\bar{T}$ and $\bar{q}_r$ should display symmetry, while $\bar{q}_z$ should exhibit anti-symmetry.

As a result, we can determine the thermal fields in the entire physical domain. Figures 6 and 7 show these fields around the crack region in both examined problems. The results are plotted for the case of $\bar{a} = 2$ and $\bar{h} = 1.5$.

In view of the symmetry characteristics of the studied problems, our discussion mainly focuses on the half-layer where $0 \le \zeta \le \bar{h}$. From Figs. 6(a) and 7(a), it can be seen that the temperature is highest on the heated boundary area ($\bar{\zeta} = 0$ and $0 \le \rho \le \bar{a}$) and decreases as ρ or ζ increases. On the other hand, the temperature remains consistently at zero in the regions $\zeta = 0$, $\rho > \bar{a}$ and $\zeta = \bar{h}$, $\rho > 1$, in accordance with the boundary conditions (2a) and (2c).

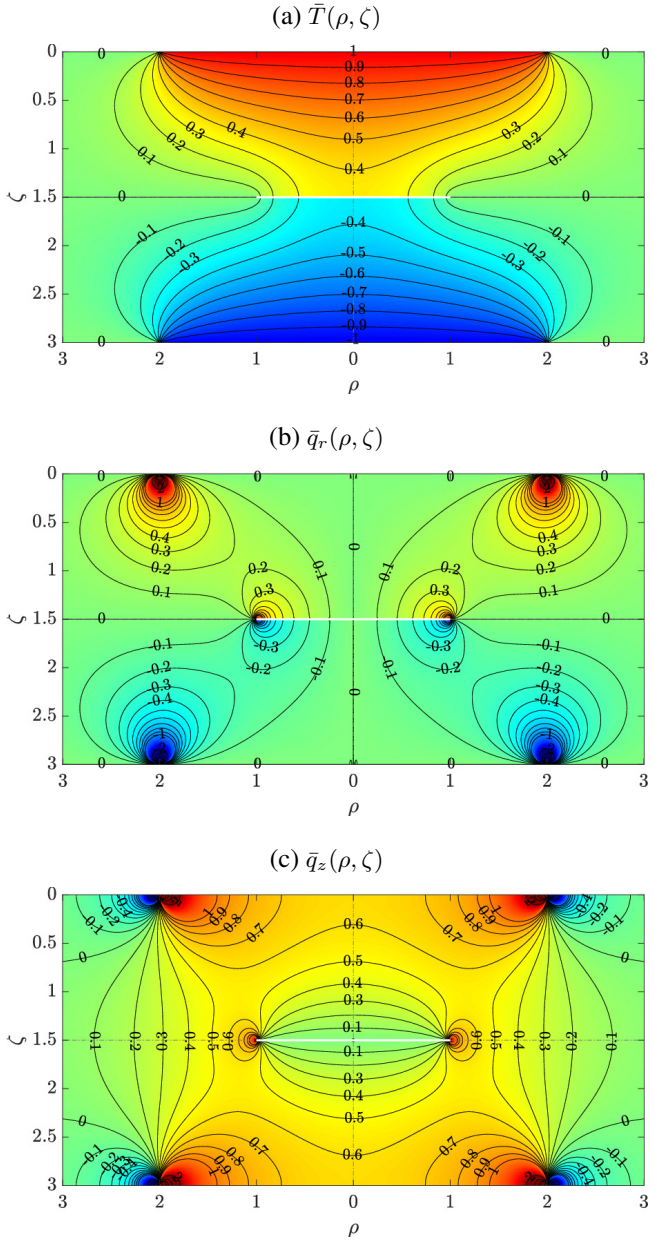

Fig. 6: Contour plots of the thermal fields around the crack region with $\bar{a} = 2$ and $\bar{h} = 1.5$ for the first problem (involving a penny-shaped crack). (a) $\bar{T}(\rho,\zeta)$; (b) $\bar{q}_r(\rho,\zeta)$; (c) $\bar{q}_z(\rho,\zeta)$.

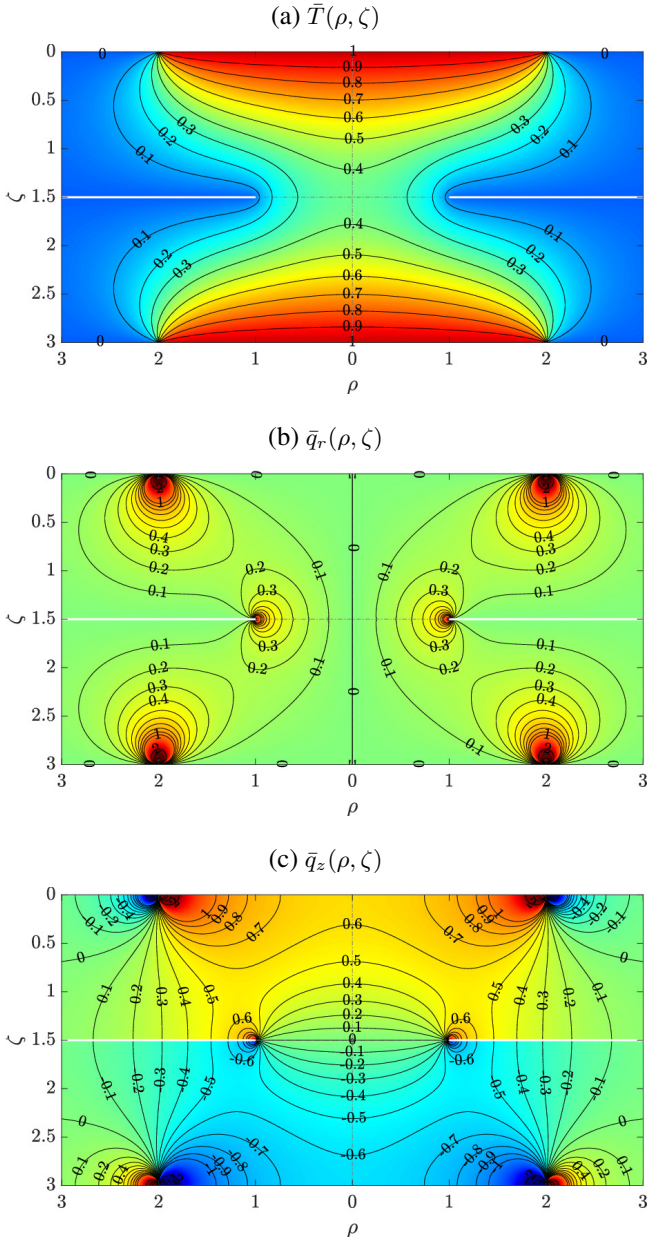

Fig. 7: Contour plots of the thermal fields around the crack region with $\bar{a} = 2$ and $\bar{h} = 1.5$ for the second problem (involving an external crack). (a) $\bar{T}(\rho,\zeta)$; (b) $\bar{q}_r(\rho,\zeta)$; (c) $\bar{q}_z(\rho,\zeta)$.

In the first problem, where the medium contains a penny-shaped crack, a temperature discontinuity is evident across the crack, as illustrated in Fig. 6(a). The temperature distributions on the lower and upper crack surfaces have equal magnitudes but opposite signs. This discontinuity reflects the heat transfer characteristics imposed by the boundary conditions and the nature of the crack. In contrast, in the second problem (the case of an external crack), the temperature in the region $\zeta = \bar{h}$, $\rho < 1$ remains continuous, as depicted in Fig. 7(a).

Figures 6(b), (c), 7(b) and (c) indicate that both heat fluxes are concentrated in the vicinity of the region $\zeta = 0$, $\rho = \bar{a}$ and near the crack tip ($\zeta = \bar{h}$, $\rho = 1$). They vary considerably around these areas and vanish as ρ becomes larger. Additionally, the heat flux in the radial direction vanishes in the median plane ($\zeta = \bar{h}$) for $\rho > 1$, as revealed in Figs. 6(b) and 7(b). These figures also show that $\bar{q}_r$ vanishes on the axis $\rho = 0$, which is consistent with the axisymmetric nature of the present problems.

Now, we investigate the effect of the dimensionless parameters $\bar{a}$ and $\bar{h}$ on the thermal fields along the crack plane. Considering the previously mentioned symmetry characteristics, we focus on the results related to the lower crack plane $\zeta = \bar{h}^-$. The variations of the dimensionless temperature $\bar{T}$ at this plane, as a function of the normalized radial coordinate ρ, are depicted in Figs. 8(a) and (b) for different values of $\bar{a}$ and $\bar{h}$, respectively.

It can be observed that, for a given $\bar{a}$ and $\bar{h}$, the temperature reaches its maximum value on the symmetry axis ($\rho = 0$) and decreases as ρ increases along the circular area of radius 1, until it vanishes at the crack tip ($\rho = 1$). On the remaining part of the crack plane ($\rho > 1$), the temperature remains consistently zero, conforming to the boundary condition (2c), which is also indicated in Figs. 6(a) and 7(a). Figure 8 also shows that, for a fixed value of $\bar{h}$, a significant temperature variation corresponds to a larger value of $\bar{a}$. Conversely, for a specific value of $\bar{a}$, notable temperature variation aligns with a smaller value of $\bar{h}$.

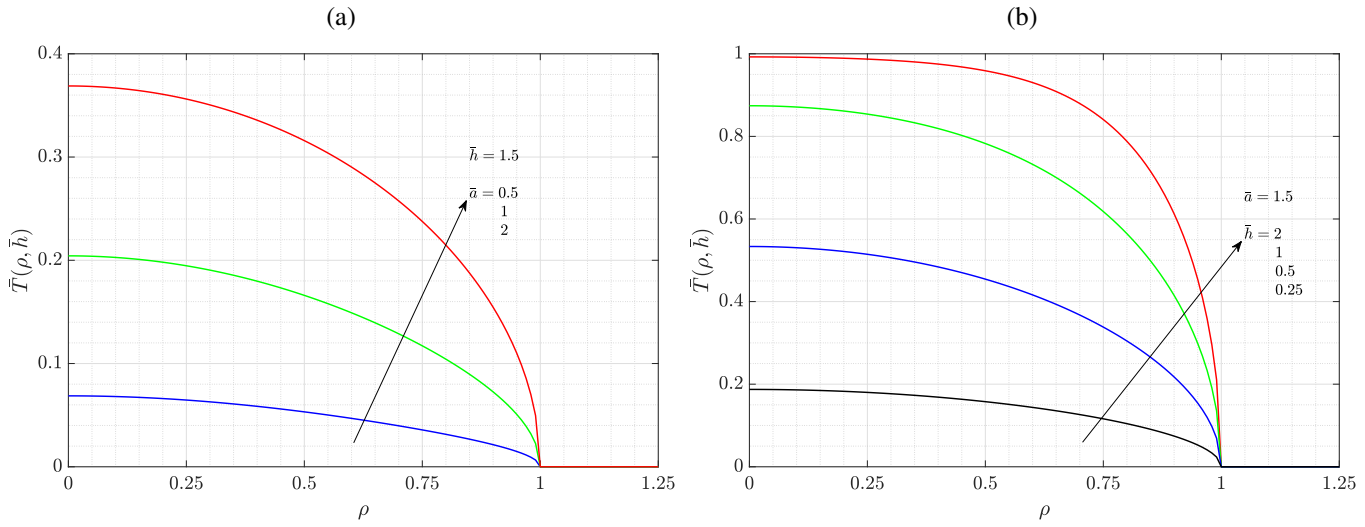

Fig. 8: Radial distribution of $\bar{T}$ on the lower crack plane ($\zeta = \bar{h}^-$) for: (a) various values of $\bar{a}$ with $\bar{h} = 1.5$; (b) different values of $\bar{h}$ with $\bar{a} = 1.5$.

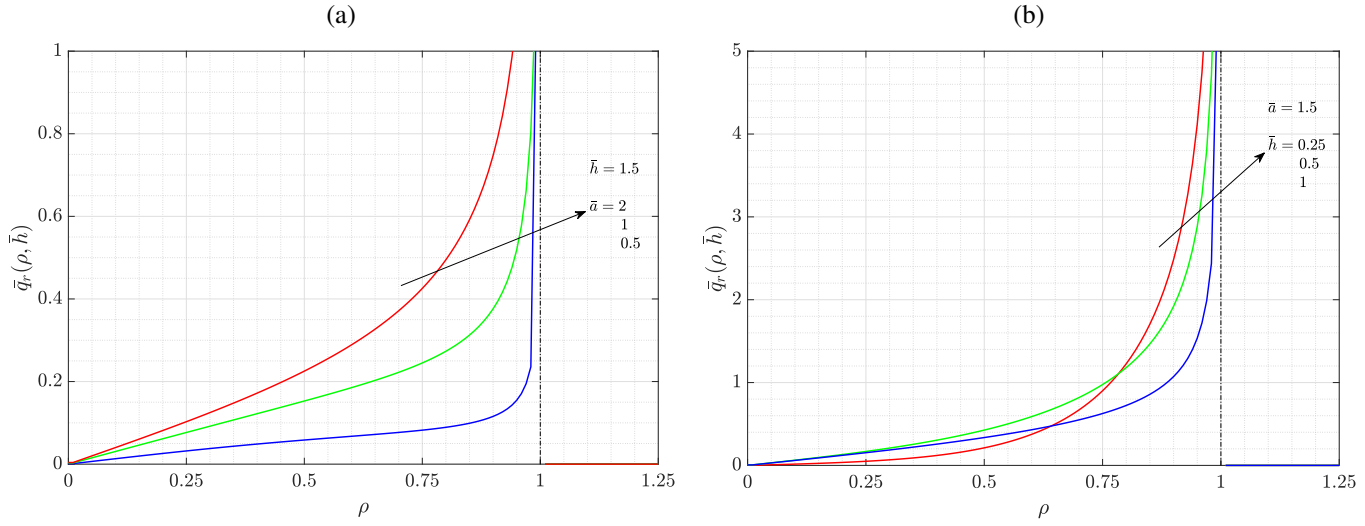

Fig. 9: Radial distribution of $\bar{q}_r$ on the lower crack plane ($\zeta = \bar{h}^-$) for: (a) various values of $\bar{a}$ with $\bar{h} = 1.5$; (b) different values of $\bar{h}$ with $\bar{a} = 1.5$.

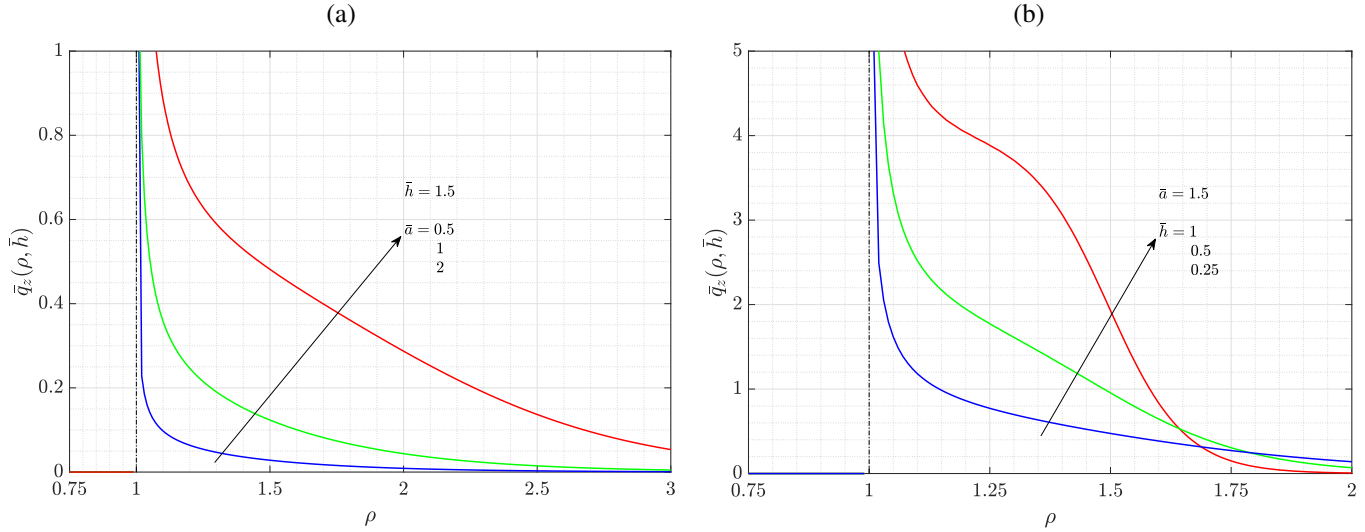

Fig. 10: Radial distribution of $\bar{q}_z$ on the lower crack plane ($\zeta = \bar{h}^-$) for: (a) various values of $\bar{a}$ with $\bar{h} = 1.5$; (b) different values of $\bar{h}$ with $\bar{a} = 1.5$.

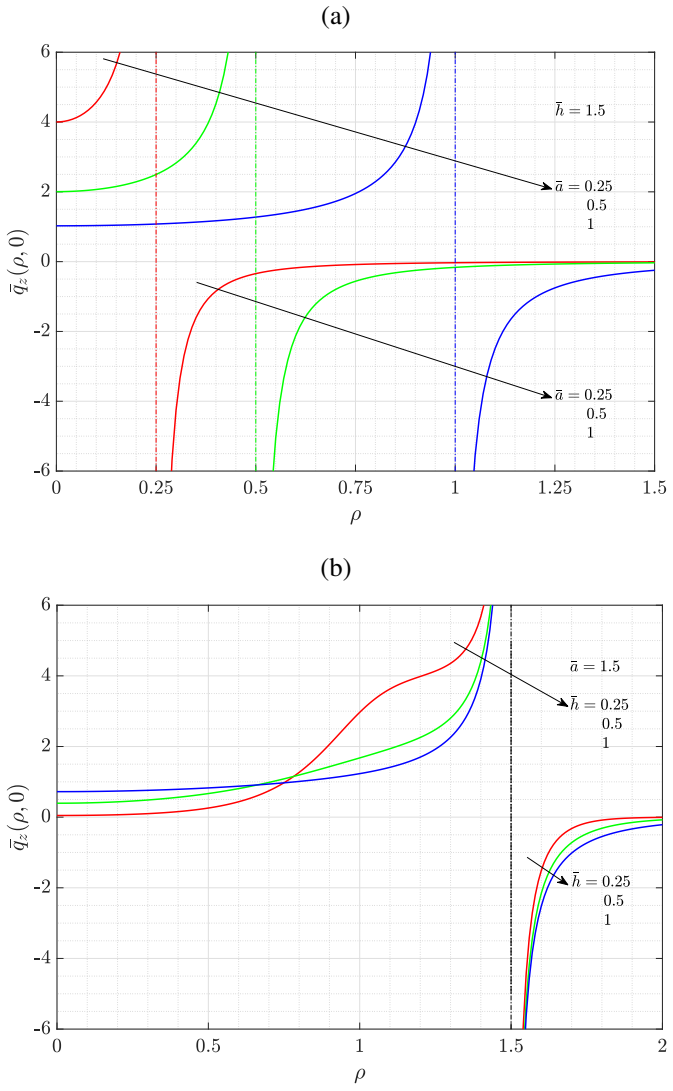

Fig. 11: Radial distribution of $\bar{q}_z$ on the external surface $\zeta = 0$ for: (a) various values of $\bar{a}$ with $\bar{h} = 1.5$; (b) different values of $\bar{h}$ with $\bar{a} = 1.5$.

Regarding the heat fluxes, Figs. 9 and 10 illustrate the distribution of $\bar{q}_r$ and $\bar{q}_z$ on the lower crack plane ($\zeta = \bar{h}^-$), respectively. The results are plotted for various values of the dimensionless parameters $\bar{a}$ and $\bar{h}$. From these figures, it is evident that both heat fluxes exhibit singular behavior near the crack tip. Specifically, the heat flux in the radial direction shows singularity in the vicinity $\rho \to 1^-$, whereas the heat flux in the axial direction displays singularity in the vicinity $\rho \to 1^+$.

Furthermore, as depicted in Fig. 9, the heat flux in the radial direction $\bar{q}_r$ vanishes at the center ($\rho = 0$), increases as ρ increases within the circular area $\rho < 1$, and exhibits significant variations in the vicinity of the crack tip ($\rho \to 1^-$). Along the remaining part of the crack plane (i.e., $\rho > 1$), $\bar{q}_r$ consistently remains zero, which is also shown in Figs. 6(b) and 7(b).

As dictated by the boundary condition (2b), the heat flux in the axial direction should vanish within the circular region $\rho < 1$. This condition is indicated in Fig. 10. It is also seen from this figure that $\bar{q}_z$ decays rapidly with increasing ρ ($\rho > 1$), eventually approaching zero as ρ becomes larger.

Moreover, Figs. 9(a) and 10(a) indicate that a larger radius $\bar{a}$ of the heated area results in larger heat fluxes on the lower crack plane. Similarly, from Figs. 9(b) and 10(b), it can be observed that as the crack is closer to the partially heated external surface ($\zeta = 0$), the heat fluxes on the lower crack plane are larger in magnitude.

The analysis of $\bar{q}_z$ variation at the plane $\zeta = 0$ is also of particular interest. The profiles of $\bar{q}_z$ along the radial direction at the external surface ($\zeta = 0$) are presented in Figs. 11(a) and (b) for different values of $\bar{a}$ and $\bar{h}$, respectively. It is clear that $\bar{q}_z$ is singular at $\rho = \bar{a}$ and varies significantly in its vicinity ($\rho \to \bar{a}^{\pm}$).

Notably, within the circular area of radius $\bar{a}$, $\bar{q}_z$ is positive, while it becomes negative on the remaining part of the external surface ($\rho > \bar{a}$). Additionally, the magnitude of $\bar{q}_z$ increases as ρ varies from 0 to $\bar{a}$. This trend also holds true for $\rho > \bar{a}$ (where $\bar{q}_z$ is negative), and it eventually tends toward zero as ρ becomes larger. Further analysis of both figures reveals that the profile of $\bar{q}_z$ varies across different combinations of $\bar{a}$ and $\bar{h}$. This difference is less noticeable when varying $\bar{h}$, especially when ρ is greater than $\bar{a}$, as shown in Fig. 11(b).

D. Heat flux intensity factor

In this subsection, we examine how the dimensionless parameters $\bar{a}$ and $\bar{h}$ influence the normalized heat flux intensity factor $\bar{K}_T$. To this end, we display in Fig. 12 a contour plot of $\bar{K}_T$ as a function of both $\bar{a}$ and $\bar{h}$. The plot is presented on a log-linear scale to better highlight the $\bar{K}_T$ variation. It is noteworthy to see from this figure that, as $\bar{a}$ increases up to 0.6, the magnitude of $\bar{K}_T$ consistently falls within the range of 0.1 to 0.2. This observation remains consistent when $\bar{a}$ exceeds 0.6, and $\bar{h}$ ranges from 3 to 5.

Additionally, for a fixed value of $\bar{h}$, the magnitude of the heat flux intensity factor rapidly increases as $\bar{a}$ rises from 0.6 to 1.2, then tends to stabilize with further increases in the value of $\bar{a}$. On the other hand, when $\bar{a}$ exceeds 1.2, $\bar{K}_T$ decreases monotonically as $\bar{h}$ increases. In other words, the closer the crack is to the external surfaces, the larger the magnitude of the heat flux intensity factor.

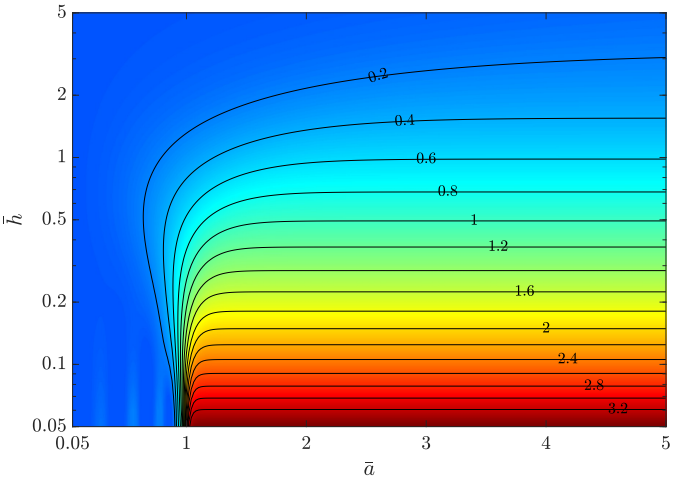

Fig. 12: Contour plot of the normalized heat flux intensity factor $\bar{K}_T$ versus $\bar{a}$ and $\bar{h}$ presented on a semi-logarithmic scale.

V. Conclusion

In this study, we investigated a heat conduction problem in a layer with prescribed temperature conditions that also containing a circular crack, either internal or external. Closed-form expressions were derived for various physical quantities, including temperature, heat fluxes, and heat flux intensity factor. Numerical results were presented to gain insight into the behavior of these quantities and their dependence on various parameters, such as the surface radius of the applied temperatures and the layer thickness.

The proposed method has demonstrated its effectiveness in solving the current heat conduction problem. Furthermore, its broad applicability extends beyond this specific case, allowing it to handle a wide range of mixed boundary value problems in the field of heat conduction, as well as in other scientific domains such as thermo-elasticity [15, 16], electrostatics [41, 42] and fluid mechanics [43, 44].

Our results may serve as valuable analytical tools for validating solutions obtained through numerical approaches. Furthermore, they can be utilized to derive thermal displacements and stresses for the corresponding thermoelastic problems, which will be addressed in future research endeavors.

Appendices

A Evaluation of the integrals

This appendix is dedicated to providing comprehensive details regarding the derivation of expressions for some integrals involved in this study.

A. $\displaystyle\int_0^\infty \xi \coth(h\,\xi)\, J_0(r\,\xi)\, J_1(a\,\xi)\,\mathrm{d}\xi$

Knowing that $\lim\limits_{\xi\to\infty} \coth(h\,\xi) = 1$, the following integral can be rewritten as

$$\begin{aligned}&\int_0^\infty \xi \coth(h\,\xi)\, J_0(r\,\xi)\, J_1(a\,\xi)\,\mathrm{d}\xi\\ &= \int_0^\infty \xi \left[\coth(h\,\xi) - 1\right] J_0(r\,\xi)\, J_1(a\,\xi)\,\mathrm{d}\xi\\ &\quad + \int_0^\infty \xi\, J_0(r\,\xi)\, J_1(a\,\xi)\,\mathrm{d}\xi.\end{aligned} \tag{A.1}$$

Making use of the identity $\xi\, J_1(\xi) = -\partial J_0(a\,\xi)/\partial a$ and changing the order of integration and derivation, we get

$$\int_0^\infty \xi\, J_0(r\,\xi)\, J_1(a\,\xi)\,\mathrm{d}\xi = -\frac{\partial}{\partial a}\int_0^\infty J_0(a\,\xi)\, J_0(r\,\xi)\,\mathrm{d}\xi. \tag{A.2}$$

By virtue of [27, Eq. (6.576 2)], the integral on the right hand side of (A.2) can be evaluated as

$$\int_0^\infty J_0(a\,\xi)\, J_0(r\,\xi)\,\mathrm{d}\xi = \frac{F\left(\frac{1}{2},\,\frac{1}{2};\,1;\,\frac{4\,r\,a}{(r+a)^2}\right)}{r+a}, \tag{A.3}$$

where F stands for the Gauss hypergeometric function defined by the following power series [27, Eq. (9.14)]

$$F(\alpha,\,\beta;\,\gamma;\,x) = \sum_{n=0}^{\infty} \frac{(\alpha)_n\,(\beta)_n}{(\gamma)_n}\,\frac{x^n}{n!}, \tag{A.4}$$

with $(\alpha)_n = \Gamma(\alpha+n)/\Gamma(\alpha)$, and $|x| < 1$. We denote by Γ the gamma function defined by $\Gamma(x) = \displaystyle\int_0^\infty t^{x-1}\,\mathrm{e}^{-t}\,\mathrm{d}t$, for $x > 0$. In addition, from [27, Eq. (8.113 1)], we have

$$F\left(\frac{1}{2},\,\frac{1}{2};\,1;\,\frac{4\,r\,a}{(r+a)^2}\right) = \frac{2}{\pi}K\left(\frac{2\sqrt{r\,a}}{r+a}\right). \tag{A.5}$$

We insert (A.5) into (A.3) and proceed with the differentiation with respect to a, using the formula $\dfrac{\mathrm{d}K(x)}{\mathrm{d}x} = \dfrac{E(x)}{x\,(1-x^2)} - \dfrac{K(x)}{x}$ [27, Eq. (8.123 2)]. The resulting equation is then introduced into (A.1), and hence, we obtain

$$\begin{aligned}&\int_0^\infty \xi \coth(h\,\xi)\, J_0(r\,\xi)\, J_1(a\,\xi)\,\mathrm{d}\xi\\ &= \int_0^\infty \xi \left[\coth(h\,\xi) - 1\right] J_0(r\,\xi)\, J_1(a\,\xi)\,\mathrm{d}\xi\\ &\quad - \frac{1}{\pi\,a}\left[\frac{E\left(\frac{2\sqrt{a\,r}}{r+a}\right)}{r-a} - \frac{K\left(\frac{2\sqrt{a\,r}}{r+a}\right)}{r+a}\right].\end{aligned} \tag{A.6}$$

Regarding the evaluation of the integral on the right-hand side of (A.6), it is worth noting that it converges rapidly. Therefore, it can be truncated to an integral from 0 to a sufficiently large number and subsequently evaluated numerically using a suitable method.

B. $\displaystyle\int_0^\infty \xi\, N_n(\xi)\, J_1(r\,\xi)\,\mathrm{d}\xi$

We use the relation $\xi\, J_1(\xi) = -\partial J_0(r\,\xi)/\partial r$ to express the considered integral as

$$\int_0^\infty \xi\, N_n(\xi)\, J_1(r\,\xi)\,\mathrm{d}\xi = -\frac{\partial}{\partial r}\int_0^\infty N_n(\xi)\, J_0(r\,\xi)\,\mathrm{d}\xi. \tag{A.7}$$

Then, with the help of (15), we get

$$\begin{aligned}&\frac{\partial}{\partial r}\int_0^\infty N_n(\xi)\, J_0(r\,\xi)\,\mathrm{d}\xi\\ &= \frac{4}{\pi\,b^2}\,\frac{\partial}{\partial r}\left[\frac{\sqrt{b^2-r^2}}{r}\,H(b-r)\,U_{2\,n+1}(r/b)\right] &\text{(A.8a)}\\ &= \frac{4}{\pi\,b^2}\left[\frac{\sqrt{b^2-r^2}}{r}\,U_{2\,n+1}(r/b)\,\frac{\partial}{\partial r}H(b-r)\right.\\ &\quad \left. + H(b-r)\,\frac{\partial}{\partial r}\left(\frac{\sqrt{b^2-r^2}}{r}\,U_{2\,n+1}(r/b)\right)\right]. &\text{(A.8b)}\end{aligned}$$

Knowing that $\partial H(b-r)/\partial r = \delta(b-r) = 0$ for $r \neq b$, and

$$\lim_{r\to b^-}\left[\frac{\sqrt{b^2-r^2}}{r}\,\delta(b-r)\,U_{2\,n+1}(r/b)\right] = 0, \tag{A.9}$$

we determine that the first term involved in (A.8b) vanishes.

On the other hand, by employing the variable change $\rho = r/b$, the remaining partial derivative involved in (A.8b) can be transformed into the following form

$$\frac{\partial}{\partial r}\left[\frac{\sqrt{b^2-r^2}}{r}\,U_{2\,n+1}(r/b)\right] = \frac{\partial}{b\,\partial\rho}\left[\frac{\sqrt{1-\rho^2}}{\rho}\,U_{2\,n+1}(\rho)\right]. \tag{A.10}$$

Before proceeding with differentiation, let us introduce the differentiation formula for the Chebyshev polynomials U_n as follows

$$\frac{\mathrm{d}}{\mathrm{d}x}\,U_n(x) = \frac{(n+1)T_{n+1}(x) - x\,U_n(x)}{x^2-1}, \tag{A.11}$$

where T_n represents Chebyshev's polynomials of the first kind of degree n, defined by [27, Eq. (8.940 1)] as $T_n(x) = \cos(n \arccos x)$. Here, it is worth mentioning that (A.11) is obtained by differentiating the polynomials in their trigonometric forms. Considering (A.11), we perform the differentiation on the right-hand side of (A.10). This operation results in

$$\frac{\partial}{\partial\rho}\left[\frac{\sqrt{1-\rho^2}}{\rho}\,U_{2\,n+1}(\rho)\right] = -\frac{2\,(n+1)\,\rho\,T_{2\,n+2}(\rho)+(1-\rho^2)U_{2\,n+1}(\rho)}{\rho^2\,\sqrt{1-\rho^2}}. \tag{A.12}$$

By making use of the following recursion formulas [27, Eq. (8.941 3 and 2)]

$$T_n(x) = U_n(x) - x\,U_{n-1}(x), \tag{A.13a}$$
$$U_{n+1}(x) - 2\,x\,U_n(x) + U_{n-1}(x) = 0, \tag{A.13b}$$

(A.12) can be expressed in terms of Chebyshev's polynomials of the second kind only, and further can be simplified to

$$\frac{\partial}{\partial\rho}\left[\frac{\sqrt{1-\rho^2}}{\rho}\,U_{2\,n+1}(\rho)\right] = \frac{2\,(n+1)\,\rho\,U_{2\,n}(\rho) - \left[(2\,n+1)\,\rho^2+1\right]U_{2\,n+1}(\rho)}{\rho^2\,\sqrt{1-\rho^2}}. \tag{A.14}$$

Hence, by inserting (A.14) into (A.10) and remembering that $\rho = r/b$, we find that

$$\frac{\partial}{\partial r}\left[\frac{\sqrt{b^2-r^2}}{r}\,U_{2\,n+1}(r/b)\right] = \frac{1}{r^2\,\sqrt{b^2-r^2}}\left\{2\,(n+1)\,b\,r\,U_{2\,n}(r/b) - \left[(2\,n+1)\,r^2+b^2\right]U_{2\,n+1}(r/b)\right\}. \tag{A.15}$$

Via substitution of (A.15) into (A.7), one finally obtains the following analytical expression for the integral under consideration

$$\int_0^\infty \xi\,N_n(\xi)\,J_1(r\,\xi)\,\mathrm{d}\xi = -\frac{4\,H(b-r)}{\pi\,b^2\,r^2\,\sqrt{b^2-r^2}}\left\{2\,(n+1)\,b\,r\,U_{2\,n}(r/b) - \left[(2\,n+1)\,r^2+b^2\right]U_{2\,n+1}(r/b)\right\}. \tag{A.16}$$

C. $\int_{\eta_0}^\infty \bar{N}_n(\eta)\,\bar{Y}_m(\eta)\,\mathrm{d}\eta$

Upon introducing the variable change $\eta = b\,\xi$, the functions $\bar{M}_n$, $\bar{X}_m$, $\bar{N}_n$, and $\bar{Y}_m$ are expressed as follows

$$\bar{M}_n(\eta) = M_n(\eta/b) = J_{n+1/2}\,(\eta/2)\;J_{-(n+1/2)}(\eta/2), \tag{A.17a}$$
$$\bar{N}_n(\eta) = \eta\left[\bar{M}_n(\eta) - \bar{M}_{n+1}(\eta)\right], \tag{A.17b}$$
$$\bar{X}_m(\eta) = X_m(\eta/b) = J_m^2\,(\eta/2), \tag{A.17c}$$
$$\bar{Y}_m(\eta) = \eta\left[\bar{X}_m(\eta) - \bar{X}_{m+2}(\eta)\right]. \tag{A.17d}$$

On the other hand, the asymptotic expansion of the Bessel function J_ν for large values of the argument x reads [27, Eq. (8.451 1)]

$$J_\nu(x) = \sqrt{\frac{2}{\pi\,x}}\left[\cos\left(x-(2\,\nu+1)\,\frac{\pi}{4}\right) - \frac{4\,\nu^2-1}{8\,x}\times\sin\left(x-(2\,\nu+1)\,\frac{\pi}{4}\right)+O\left(\frac{1}{x^2}\right)\right]. \tag{A.18}$$

We then use (A.18) along with the trigonometric identities below

$$\begin{aligned}
&\cos(x)\;\cos(y) = \left[\cos(x+y)+\cos(x-y)\right]/2,\\
&\cos(x)\;\sin(y) = \left[\sin(x+y)-\sin(x-y)\right]/2,\\
&\cos(x+y) = \cos(x)\;\cos(y)-\sin(x)\;\sin(y),\\
&\sin(x+y) = \cos(x)\;\sin(y)+\sin(x)\;\cos(y),
\end{aligned} \tag{A.19}$$

to get the following asymptotic expansions of $\bar{M}_n$ and $\bar{X}_m$

$$\bar{M}_n(\eta) = \frac{2}{\pi\,\eta}\left[\sin(\eta)+\frac{2\,n\,(n+1)\,\cos(\eta)}{\eta}\right]+O\left(\frac{1}{\eta^3}\right), \tag{A.20a}$$

$$\bar{X}_m(\eta) = \frac{2}{\pi\,\eta}\left[1+(-1)^m\,\sin(\eta)+(-1)^m \times\left(4\,m^2-1\right)\frac{\cos(\eta)}{2\,\eta}\right]+O\left(\frac{1}{\eta^3}\right). \tag{A.20b}$$

Substituting (A.20a) and (A.20b) into (A.17b) and (A.17d), respectively, with some algebraic manipulations, we obtain

$$\bar{N}_n(\eta) = -\frac{8\,(n+1)\,\cos(\eta)}{\pi\,\eta}+O\left(\frac{1}{\eta^2}\right), \tag{A.21a}$$

$$\bar{Y}_m(\eta) = -\frac{16\,(-1)^m\,(m+1)\,\cos(\eta)}{\pi\,\eta}+O\left(\frac{1}{\eta^2}\right). \tag{A.21b}$$

By virtue of (A.21), the following integral can be approximated as

$$\int_{\eta_0}^\infty \bar{N}_n(\eta)\,\bar{Y}_m(\eta)\,\mathrm{d}\eta \simeq \frac{128\,(-1)^m\,(m+1)\,(n+1)}{\pi^2}\times\int_{\eta_0}^\infty\frac{\cos(\eta)^2}{\eta^2}\,\mathrm{d}\eta. \tag{A.22}$$

We shall proceed to perform integration by parts on the right-hand side of (A.22). Given that $\left.\frac{\cos(\eta)^2}{\eta}\right|_{\eta_0}^{\infty} = -\frac{\cos(\eta_0)^2}{\eta_0}$ and the identity $2\,\cos x\,\sin x = \sin 2\,x$, one gets

$$\int_{\eta_0}^\infty\frac{\cos(\eta)^2}{\eta^2}\,\mathrm{d}\eta = \frac{\cos(\eta_0)^2}{\eta_0}+\mathrm{si}(2\,\eta_0), \tag{A.23}$$

where si is the sine integral function defined previously by (51). Finally, inserting (A.23) into (A.22), yields

$$\int_{\eta_0}^\infty \bar{N}_n(\eta)\,\bar{Y}_m(\eta)\,\mathrm{d}\eta \simeq \frac{128\,(-1)^m\,(m+1)\,(n+1)}{\pi^2}\times\left[\frac{\cos(\eta_0)^2}{\eta_0}+\mathrm{si}(2\,\eta_0)\right]. \tag{A.24}$$

D. $\int_0^\infty \xi\coth(h\,\xi)\,N_n(\xi)\,J_0(r\,\xi)\,\mathrm{d}\xi$

From (A.21a), we have

$$N_n(\xi) = \frac{\bar{N}_n(b\,\xi)}{b} \sim -\frac{8\,(n+1)\,\cos(b\,\xi)}{\pi\,b^2\,\xi},\quad \text{as}\quad \xi\to\infty. \tag{A.25}$$

Knowing that $\lim_{\xi\to\infty}\coth(h\,\xi) = 1$, we get

$$\int_0^\infty \xi\coth(h\,\xi)\,N_n(\xi)\,J_0(r\,\xi)\,\mathrm{d}\xi = \int_0^\infty\left[\xi\coth(h\,\xi)\,N_n(\xi)+\frac{8\,(n+1)\,\cos(b\,\xi)}{\pi\,b^2}\right]\times J_0(r\,\xi)\,\mathrm{d}\xi - \frac{8\,(n+1)}{\pi\,b^2}\int_0^\infty\cos(b\,\xi)\,J_0(r\,\xi)\,\mathrm{d}\xi. \tag{A.26}$$

Recalling the relation [27, Eq. (6.671 2)], yields

$$\int_0^\infty \cos(b\,\xi)\,J_0(r\,\xi)\,\mathrm{d}\xi = \frac{1}{\sqrt{r^2-b^2}}, \qquad r > b. \tag{A.27}$$

Finally, after substitution of (A.27) into (A.26), the resulting expression is

$$\begin{aligned}&\int_0^\infty \xi\coth(h\,\xi)\,N_n(\xi)\,J_0(r\,\xi)\,\mathrm{d}\xi\\ &= \int_0^\infty \left[\xi\coth(h\,\xi)\,N_n(\xi) + \frac{8\,(n+1)\cos(b\,\xi)}{\pi\,b^2}\right]\\ &\quad\times J_0(r\,\xi)\,\mathrm{d}\xi - \frac{8\,(n+1)}{\pi\,b^2\,\sqrt{r^2-b^2}}.\end{aligned} \tag{A.28}$$

B Exact solution for the half-space case ($h \to \infty$)

In this appendix, we present an exact solution for a steady-state heat conduction problem within a semi-infinite medium. This medium is exposed to a constant temperature over a circular region on its external surface. The corresponding governing equation is given by (1), and it is subject to the boundary condition (2a). In addition, the regularity condition requires the thermal fields to vanish at infinity ($\sqrt{r^2+z^2} \to \infty$).

By following the same solution procedure presented in the subsection III.*A*, one obtains

$$T_H(\xi, z) = \frac{\mathrm{e}^{-z\,\xi}\,A(\xi)}{\xi}, \tag{B.1}$$

where A denotes an unknown function. Then, Applying the boundary condition (2a) and Hankel transform theorem, we obtain

$$A(\xi) = a\,T_0\,J_1(a\,\xi). \tag{B.2}$$

Substituting (B.2) into (B.1) and performing the Hankel inversion transform given by (3b) yields the explicit formula below

$$T = a\,T_0\int_0^\infty \mathrm{e}^{-z\,\xi}\,J_0(r\,\xi)\,J_1(a\,\xi)\,\mathrm{d}\xi. \tag{B.3}$$

Subsequently, the following expressions for heat fluxes are derived

$$q_r = a\,k\,T_0\int_0^\infty \xi\,\mathrm{e}^{-z\,\xi}\,J_1(a\,\xi)\,J_1(r\,\xi)\,\mathrm{d}\xi, \tag{B.4a}$$

$$q_z = a\,k\,T_0\int_0^\infty \xi\,\mathrm{e}^{-z\,\xi}\,J_0(r\,\xi)\,J_1(a\,\xi)\,\mathrm{d}\xi. \tag{B.4b}$$

Acknowledgement

The support from Directorate-General for Scientific Research and Technological Development (DG-RSDT) of Algerian government in the form of research grant is gratefully acknowledged. The Laboratory of Green and Mechanical Development (LGMD) of National Polytechnic School (ENP) is also gratefully acknowledged for the resources and support.

References

[1] K. Cole, J. Beck, A. Haji-Sheikh, and B. Litkouhi, *Heat conduction using Greens functions*. New York: CRC Press, 2010.

[2] D. W. Hahn and M. N. Özisik, *Heat conduction*. New Jersey: John Wiley & Sons, 2012.

[3] S. Kakaç, Y. Yener, and C. P. Naveira-Cotta, *Heat conduction*. New York: CRC Press, 2018.

[4] R. S. Dhaliwal, "Mixed boundary value problem of heat conduction for infinite slab," *Applied Scientific Research*, vol. 16, no. 1, pp. 228–240, 1966. doi: 10.1007/BF00384070

[5] R. S. Dhaliwal, "An axisymmetric mixed boundary value problem for a thick slab," *SIAM Journal on Applied Mathematics*, vol. 15, no. 1, pp. 98–106, 1967. doi: 10.1137/0115006

[6] J. V. Beck, "Large time solutions for temperatures in a semi-infinite body with a disk heat source," *International Journal of Heat and Mass Transfer*, vol. 24, no. 1, pp. 155–164, 1981. doi: 10.1016/0017-9310(81)90104-6

[7] R. C. Mehta and T. K. Bose, "Temperature distribution in a large circular plate heated by a disk heat source," *International Journal of Heat and Mass Transfer*, vol. 26, no. 7, pp. 1093–1095, 1983. doi: 10.1016/S0017-9310(83)80136-7

[8] G. M. L. Gladwell, J. R. Barber, and Z. Olesiak, "Thermal problems with radiation boundary conditions," *The Quarterly Journal of Mechanics and Applied Mathematics*, vol. 36, no. 3, pp. 387–401, 1983. doi: 10.1093/qjmam/36.3.387

[9] T. F. Lemczyk and M. M. Yovanovich, "Thermal constriction resistance with convective boundary conditions—1. half-space contacts," *International Journal of Heat and Mass Transfer*, vol. 31, no. 9, pp. 1861–1872, 1988. doi: 10.1016/0017-9310(88)90200-1

[10] T. F. Lemczyk and M. M. Yovanovich, "Thermal constriction resistance with convective boundary conditions—2. layered half-space contacts," *International Journal of Heat and Mass Transfer*, vol. 31, no. 9, pp. 1873–1883, 1988. doi: 10.1016/0017-9310(88)90201-3

[11] T. V. Rao, "Effect of surface layers on the constriction resistance of an isothermal spot. part I: Reduction to an integral equation and numerical results," *Heat and Mass Transfer*, vol. 40, no. 6-7, pp. 439–453, 2004. doi: 10.1007/s00231-003-0490-4

[12] T. V. Rao, "Effect of surface layers on the constriction resistance of an isothermal spot. part II: Analytical results for thick layers," *Heat and Mass Transfer*, vol. 40, no. 6-7, pp. 455–466, 2004. doi: 10.1007/s00231-003-0491-3

[13] N. Laraqi, E.-K. Chahour, E. Monier-Vinard, N. Fahdi, C. Zerbini, and M.-N. Nguyen, "Simple and accurate correlations for some problems of heat conduction with nonhomogeneous boundary conditions," *Thermal Science*, vol. 21, no. 1 Part A, pp. 125–132, 2017. doi: 10.2298/TSCI160411243L

[14] X.-F. Li and K. Y. Lee, "Effect of heat conduction of penny-shaped crack interior on thermal stress intensity factors," *International Journal of Heat and Mass Transfer*, vol. 91, pp. 127–134, 2015. doi: 10.1016/j.ijheatmasstransfer.2015.07.087

[15] X.-Y. Li, P.-D. Li, G.-Z. Kang, W.-Q. Chen, and R. Müller, "Steady-state thermo-elastic field in an infinite medium weakened by a penny-shaped crack: Complete and exact solutions," *International Journal of Solids and Structures*, vol. 84, pp. 167–182, 2016. doi: 10.1016/j.ijsolstr.2016.02.001

[16] P.-D. Li, X.-Y. Li, and G.-Z. Kang, "Axisymmetric thermo-elastic field in an infinite space containing a penny-shaped crack under a pair of symmetric uniform heat fluxes and its applications," *International Journal of Mechanical Sciences*, vol. 115, pp. 634–644, 2016. doi: 10.1016/j.ijmecsci.2016.07.027

[17] B. Kebli and Z. Baka, "Annular crack in a thermoelastic half-space," *Journal of Thermal Stresses*, vol. 43, no. 11, pp. 1379–1414, 2020. doi: 10.1080/01495739.2020.1782294

[18] J. Wang, M. Dai, and C.-F. Gao, "The effect of interfacial thermal resistance on interface crack subjected to remote heat flux," *Zeitschrift für angewandte Mathematik und Physik*, vol. 71, no. 12, pp. 1–21, 2020. doi: 10.1007/s00033-019-1235-7

[19] G. C. Sih, "Heat conduction in the infinite medium with lines of discontinuities," *Journal of Heat Transfer*, vol. 87, no. 2, pp. 293–298, 1965. doi: 10.1115/1.3689092

[20] C. Chao and R. Chang, "Steady-state heat conduction problem of the interface crack between dissimilar anisotropic media," *International Journal of Heat and Mass Transfer*, vol. 36, no. 8, pp. 2021–2026, 1993. doi: 10.1016/S0017-9310(05)80133-4

[21] D. Y. Tzou, "The singular behavior of the temperature gradient in the vicinity of a macrocrack tip," *International Journal of Heat and Mass Transfer*, vol. 33, no. 12, pp. 2625–2630, 1990. doi: 10.1016/0017-9310(90)90198-4

[22] T.-C. Chiu, S.-W. Tsai, and C.-H. Chue, "Heat conduction in a functionally graded medium with an arbitrarily oriented crack," *International Journal of Heat and Mass Transfer*, vol. 67, pp. 514–522, 2013. doi: 10.1016/j.ijheatmasstransfer.2013.08.022

[23] S.-W. Tsai, T.-C. Chiu, and C.-H. Chue, "Temperature distribution and heat flow around a crack of arbitrary orientation in a functionally graded medium," *Journal of Engineering Mathematics*, vol. 87, no. 1, pp. 123–137, 2014. doi: 10.1007/s10665-013-9664-3

[24] H. Deng, B. Yan, H. Su, X. Zhang, and X. Lv, "An interaction integral method for calculating heat flux intensity factor with the XFEM," *International Journal of Thermal Sciences*, vol. 136, pp. 379–388, 2019. doi: 10.1016/j.ijthermalsci.2018.09.022

[25] H. Deng, B. Yan, H. Su, X. Zhang, and X. Lv, "Study on transient heat flux intensity factor with interaction integral," *International Journal of Thermal Sciences*, vol. 146, p. 106014, 2019. doi: 10.1016/j.ijthermalsci.2019.106014

[26] L. Debnath and D. Bhatta, *Integral transforms and their applications*. New York: Chapman and Hall/CRC, 2015.

[27] I. S. Gradshteyn and I. M. Ryzhik, *Table of integrals, series, and products*. London: Academic press, 2014.

[28] I. N. Sneddon, "The elementary solution of dual integral equations," *Glasgow Mathematical Journal*, vol. 4, no. 3, pp. 108–110, 1960. doi: 10.1017/S2040618500034006

[29] I. N. Sneddon, *Mixed boundary value problems in potential theory*. North-Holland, 1966.

[30] D. G. Duffy, *Mixed boundary value problems*. New York: CRC Press, 2008.

[31] M. Sakamoto, "An elastic layer with a penny-shaped crack subjected to internal pressure," *JSME International Journal, Series A, Solid Mechanics and Material Engineering*, vol. 46, no. 1, pp. 10–14, 2003. doi: 10.1299/jsmea.46.10

[32] B. Kebli and F. Madani, "The Reissner-Sagoci problem for an interfacial crack in an elastic bilayer medium under torsion of an embedded rigid circular disc," *Theoretical and Applied Fracture Mechanics*, vol. 110, 2020. doi: 10.1016/j.tafmec.2020.102825

[33] K. Miura, M. Sakamoto, and Y. Tanabe, "Analytical solution of axisymmetric indentation of multi-layer coating on elastic substrate body," *Acta Mechanica*, vol. 231, pp. 4077–4093, 2020. doi: 10.1007/s00707-020-02752-1

[34] K. Miura, M. Sakamoto, and Y. Tanabe, "Analytical solution for the axisymmetric problem of a penny-shaped crack under internal pressure in a multi-layer composite," *Mechanical Engineering Journal*, vol. 8, no. 2, 2021. doi: 10.1299/mej.21-00025

[35] K. Miura, C. Oyama, M. Sakamoto, and Y. Tanabe, "Indentation method accounting for thickness effect of viscoelastic layer," *ZAMM-Journal of Applied Mathematics and Mechanics/Zeitschrift für Angewandte Mathematik und Mechanik*, vol. 101, no. 10, 2021. doi: 10.1002/zamm.202000272

[36] B. Kebli and A. Gouadria, "Axisymmetric torsion problem by a rigid disc of an elastic half-space weakened by an annular crack," *Theoretical and Applied Fracture Mechanics*, vol. 123, 2023. doi: 10.1016/j.tafmec.2022.103676

[37] Z. Baka and B. Kebli, "Heat conduction problem for a half-space medium containing a penny-shaped crack," *Archive of Applied Mechanics*, vol. 93, no. 2, pp. 635–662, 2023. doi: 10.1007/s00419-022-02291-2

[38] I. Sevostianov, "Thermal conductivity of a material containing cracks of arbitrary shape," *International Journal of Engineering Science*, vol. 44, no. 8-9, pp. 513–528, 2006. doi: 10.1016/j.ijengsci.2006.04.001

[39] R. Li, Y. Zhong, B. Tian, and Y. Liu, "On the finite integral transform method for exact bending solutions of fully clamped orthotropic rectangular thin plates," *Applied Mathematics Letters*, vol. 22, no. 12, pp. 1821–1827, 2009. doi: 10.1016/j.aml.2009.07.003

[40] Y. Zhong and Q. Xu, "Analysis bending solutions of clamped rectangular thick plate," *Mathematical Problems in Engineering*, vol. 2017, 2017. doi: 10.1155/2017/7539276

[41] S. Choo, M. Leong, and W. Low, "The contact resistance at the interface between a disc electrode and an infinite slab: Mixed-boundary-value solutions," *Solid-State Electronics*, vol. 29, no. 5, pp. 535–543, 1986. doi: 10.1016/0038-1101(86)90075-4

[42] K. Seki, "Quantifying the spreading currents over the circular contact region in a good conducting cover layer on a substrate," *Journal of Physics D: Applied Physics*, vol. 53, no. 43, p. 435103, 2020. doi: 10.1088/1361-6463/ab9e37

[43] J. P. Tanzosh and H. A. Stone, "Transverse motion of a disk through a rotating viscous fluid," *Journal of Fluid Mechanics*, vol. 301, p. 295–324, 1995. doi: 10.1017/S0022112095003909

[44] A. M. Davis and S. G. L. Smith, "Tangential oscillations of a circular disk in a viscous stratified fluid," *Journal of Fluid Mechanics*, vol. 656, pp. 342–359, 2010. doi: 10.1017/S0022112010001205

Zakaria Baka received his Engineering, Master's, and Ph.D. degrees in Mechanical Engineering from the Ecole Nationale Polytechnique (ENP), Algiers, Algeria, in 2013, 2014, and 2024, respectively. He is currently conducting research at the Laboratory of Green and Mechanical Development (LGMD), ENP. His research interests include engineering mechanics, solid mechanics, heat transfer, elasticity, and thermo-elasticity.

Belkacem Kebli is a full Professor at the Department of Mechanical Engineering at the Ecole Nationale Polytechnique (ENP), Algiers, Algeria. He received High Studies Diploma (DES) in Functional Analysis from Ferhat Abbas University, Setif in 1986, and Ph. D. degree in Physics and Mathematics from Mechnikov University, Odessa in 1991. His main research interests include Elasticity theory, Fracture mechanics, and both Analytical and Numerical solutions of PDEs.